TU Delft

Delft University of Technology

Document Version
Final published version

Licence
Dutch Copyright Act (Article 25fa)

Citation (APA)
Yang, S., Correia, G. H. D. A., Wu, J., & Sun, H. (2026). Optimizing electric carsharing system operations and battery management: Integrating V2G, B2G and battery swapping strategies. *Transportation Research Part B: Methodological*, *209*, Article 103462. https://doi.org/10.1016/j.trb.2026.103462

Important note
To cite this publication, please use the final published version (if applicable).
Please check the document version above.

Copyright
In case the licence states “Dutch Copyright Act (Article 25fa)”, this publication was made available Green Open Access via the TU Delft Institutional Repository pursuant to Dutch Copyright Act (Article 25fa, the Taverne amendment). This provision does not affect copyright ownership.
Unless copyright is transferred by contract or statute, it remains with the copyright holder.

Sharing and reuse
Other than for strictly personal use, it is not permitted to download, forward or distribute the text or part of it, without the consent of the author(s) and/or copyright holder(s), unless the work is under an open content license such as Creative Commons.

Takedown policy
Please contact us and provide details if you believe this document breaches copyrights.
We will remove access to the work immediately and investigate your claim.

This work is downloaded from Delft University of Technology.

Transportation Research Part B 209 (2026) 103462

Contents lists available at ScienceDirect

Transportation Research Part B

journal homepage: www.elsevier.com/locate/trb

Optimizing electric carsharing system operations and battery management: Integrating V2G, B2G and battery swapping strategies

Shuang Yang [a], Gonçalo Homem de Almeida Correia [b], Jianjun Wu [c], Huijun Sun [a,*]

[a] School of Systems Science, Beijing Jiaotong University, Beijing, China
[b] Department of Transport & Planning, Delft University of Technology, Delft, Netherlands
[c] School of Economics & Management, Dalian University of Technology, Dalian, China

ARTICLE INFO

Keywords:
Shared electric vehicles
Recharging strategy
Energy selling
Battery swapping
Column generation
Rolling horizon approach

ABSTRACT

Shared electric vehicles (SEVs) have emerged as a promising solution for promoting sustainable urban mobility. However, ensuring the efficient operation and effective battery management of SEV systems remains a complex challenge. To address this issue, this paper introduces an integrated optimization framework for SEV systems that jointly considers Vehicle-to-Grid (V2G), Battery-to-Grid (B2G), plug-in charging, and battery swapping. The proposed approach is built on a space-time-energy network model that simultaneously optimizes battery charging and discharging scheduling together with SEV operations, such as relocations and battery swapping. The objective is to maximize profit while addressing operational constraints and the complexities of energy management within SEV systems. Given the substantial complexity of large-problem scales, the paper introduces a column generation-based heuristic algorithm. Additionally, a rolling horizon approach is employed to enable real-time decision-making under dynamic operational conditions. Extensive experiments are conducted to evaluate the effects of key parameters, such as the rolling horizon settings, charging rates, fleet sizes, and the number of stocked batteries. The effectiveness of various energy management strategies is also assessed, ranging from plug-in charging alone to its combinations with battery swapping, V2G, and B2G. Numerical results show that under low carsharing rental demand scenarios, plug-in charging alone is a cost-effective option. Moreover, battery swapping is found to be particularly effective as an auxiliary recharging method when the SEV fleet is limited, charging rates are low, or carsharing demand is high. Overall, this study provides theoretical foundations for the integration of vehicle operations and energy management in shared electric mobility systems.

1. Introduction

Carsharing services, as a form of vehicle rental, offer citizens the opportunity to use vehicles without the burden of ownership. The entire process, ranging from reserving the vehicle to its collection, return and billing, is typically handled through a user-friendly mobile app. This concept not only liberates users from the financial burdens linked with vehicle ownership, such as insurance premiums and parking expenditures, but also provides flexibility and convenience, contributing to its rapid growth (Mounce and Nelson, 2019). Consequently, carsharing holds great promise as one of the preferred travel modes in the future.

* Corresponding author.
E-mail address: hjsun1@bjtu.edu.cn (H. Sun).

https://doi.org/10.1016/j.trb.2026.103462
Received 20 September 2023; Received in revised form 19 January 2026; Accepted 23 March 2026
Available online 8 April 2026
0191-2615/© 2026 Elsevier Ltd. All rights are reserved, including those for text and data mining, AI training, and similar technologies.

In recent years, the urgency to reduce greenhouse gas emissions has intensified due to the worsening environmental crisis. Electric vehicles (EVs) are widely recognized as an effective pathway to reducing fossil fuel consumption, emissions, and energy costs in the transport sector (Rupp et al., 2019). Empirical studies show that EV deployment, together with appropriate charging strategies, can reduce greenhouse gas emissions by 3.6%-32% (Van Fan et al., 2022; Albrechtowicz, 2023). Moreover, EVs achieve a tank-to-wheel efficiency of approximately 64%, substantially exceeding the 20%-30% efficiency of conventional internal combustion engine vehicles (Albrechtowicz, 2023). These combined advantages have driven governments worldwide to implement targeted policies to accelerate EV adoption.

The use of electric mobility and carsharing has resulted in a symbiotic integration. Shared electric vehicles (SEVs) integrate the convenience and accessibility intrinsic to carsharing with the ecological benefits of EVs. The combination represents a significant step toward creating a more sustainable and efficient transportation system. Many carsharing companies have already channeled investments into the operation of SEVs, like EVCARD in China and Zity in Europe. However, the growth of SEVs faces challenges arising from the inherent limitations of EVs. Range anxiety and long charging times, particularly when using slow and cheaper charging solutions, are major issues in the operation of SEVs.

To improve the operational efficiency, operators must optimize the energy replenishment process to ensure that EVs are charged in a timely manner. Currently, there are two primary methods of recharging EVs: battery swapping and plug-in charging. Plug-in charging dominates in practice due to its cost-effectiveness and adaptability. However, it is not devoid of limitations, notably the long charging times, even when utilizing fast charging technologies. Conversely, battery swapping offers the distinct advantage of quickly replacing depleted batteries with fully charged batteries for vehicles, making it suitable for long-distance travel or emergency situations. The advent of battery swapping has revolutionized the replenishment time for EVs, aligning it with the rapid refueling capabilities of conventional fossil-fuel vehicles. Such efficiency is particularly critical for time-sensitive services like carsharing. As a result, battery swapping is increasingly regarded as a complementary solution to plug-in charging. Moreover, carsharing platforms are innately well-suited to facilitate battery pack standardization, as they can enforce uniform battery pack requirements across their fleet. Currently, some shared mobility companies such as Zbee and Gogoro, have embraced battery swapping services. Despite these advancements, as we will elaborate, there remains a significant gap in the development of comprehensive models that incorporate both recharging techniques and their integration within SEV operations.

As dependence on the power grid continues to grow, the grid is under increasing strain, particularly during peak periods. To address the challenges posed by peak-load demand, many governments have implemented demand-side management policies such as time-of-use pricing, which raises electricity prices during peak hours to incentivize load shifting. Furthermore, in this context, EVs can also contribute to energy management through vehicle-to-grid (V2G) technology. V2G is a bidirectional energy exchange system that enables EVs to feed stored energy back into the grid and draw energy from the grid when needed. During peak grid demands, EVs can discharge energy into the grid, easing power demand pressures. In addition to balancing supply and demand, V2G contributes to overall power system security by improving efficiency and operational reliability (Sturmberg et al., 2024; Wenlong et al., 2026). Another innovation is the direct bidirectional connection of batteries to the grid, termed Battery-to-Grid (B2G), which functions independently of EVs. V2G and B2G yield several benefits such as saving costs of EV owners, and enhancing the flexibility and grid stabilization (Noel et al., 2019; Liao et al., 2021).

If SEVs are equipped with V2G and their batteries with B2G, SEVs and batteries have the potential not only to enhance grid stability but also generate additional revenue for operators. This integration brings forth a scenario where EVs and batteries simultaneously participate in both the carsharing service system and the power transmission system. Within this context, the complicated coupling of users, SEVs and batteries presents a great operational challenge for operators. Mishandling this complex interaction may result in reduced system efficiency, diminished user satisfaction, and a decline in profit. As a result, effectively coordinating the scheduling of SEVs and batteries, while considering this intricate interrelationship, becomes crucial. Unfortunately, few studies have attempted to solve such a practical problem.

Another widely recognized challenge in carsharing systems, especially within one-way systems, is the issue of vehicle imbalance (Lu et al., 2021; Huang et al., 2018). One-way systems provide users with the flexibility to pick up and return vehicles at different locations. However, due to fluctuations in demand, it is common to encounter situations where some stations suffer vehicle shortages while others have surpluses. Such an imbalance negatively affects vehicle utilization. In response to this challenge, vehicle relocation has emerged as a widely recognized and effective strategy. The process involves moving excess vehicles from stations with high inventories to those experiencing shortages, thereby achieving a more balanced distribution of vehicles. In order to maximize system efficiency, vehicle relocation should be jointly optimized with recharging operations. Without coordinated optimization, simply relocating vehicles might inadvertently delay recharging and potentially affect the overall system efficiency. This integration can potentially improve the utilization rate of recharging infrastructure and increase the vehicle availability.

With the advancement of internet technologies, SEV systems operate on digital platforms, allowing users to request rides at any time via smartphones. Reservation methods vary across companies and can be categorized into advanced and instant reservations. Advanced reservations require a cut-off time, such as one day, providing operators with sufficient information for informed decision-making. In comparison, instant reservations offer greater flexibility as they allow users to send requests shortly before their intended departure time. This flexibility, however, introduces optimization challenges, as new requests must be managed in real time alongside ongoing vehicle and battery schedules. Operators must dynamically decide which new requests to serve and how to allocate SEV and battery activities while considering external factors such as grid fluctuations and vehicle travel time influenced by traffic conditions. Without an effective dynamic strategy, instant reservation systems may fail to respond efficiently to time-varying demand.

To address the above issues, this study proposes a space-time-energy network flow model to optimize coordinated operational decisions, including SEV charging and discharging, battery swapping for both vehicles and batteries, and SEV relocation. The proposed

framework integrates multiple energy management strategies, including plug-in charging, battery swapping, Vehicle-to-Grid (V2G), and Battery-to-Grid (B2G). Recognizing the computational complexity of this model, we introduce a column-generation-based (CG-based) heuristic algorithm. To enable real-time decision-making, a rolling horizon optimization framework is employed. To validate the proposed model and algorithm, we conduct numerical experiments and sensitivity analyses.

This paper is organized as follows: Section 2 provides an overview of related work and highlights the contributions of this paper. This is followed by Section 3, where the formulation of the proposed optimization model based on the space-time-energy network flow model is introduced. Section 4 outlines our solution methods including the rolling horizon framework and CG-based solution approach, designed to efficiently solve the proposed model. To assess computational efficiency and gain insights into system operations, we conduct numerical experiments in Section 5. Lastly, Section 6 provides the main conclusions from the study and outlines potential directions for future research.

2. Literature review

We review the related literature on the topics of SEVs and battery swapping. This review aims to not only provide an up-to-date and comprehensive understanding of the methodologies for addressing operational problems of SEVs and battery swapping but also shed light on areas where further investigation is needed, clearly positioning the scope and focus of the present study.

2.1. Shared electric vehicles

2.1.1. Operational problems of shared electric vehicles

In recent years, shared electric mobility has drawn growing attention. The existing literature on the topic of SEVs is extensive and can be broadly categorized into strategic-level and operational-level studies (Ait-Ouahmed et al., 2018; Liu et al., 2022; Boyacı et al., 2015). Strategic-level research focuses on long-term planning strategies, including the number, locations, capacities of parking and charging stations, as well as fleet sizes (Xu et al., 2018; Li et al., 2016; Zhao et al., 2021). As this study focuses specifically on operational-level challenges, we do not address strategic planning considerations in detail. For comprehensive discussions of strategic decision-making in SEV systems, readers are referred to the review by Yao et al. (2022).

At the operational level, studies concentrate on the daily management and operational problems, particularly concerning relocation and charging operations. Often, these two issues are addressed simultaneously in the literature. An inherent concern within one-way station-based systems is vehicle imbalance, which refers to the imbalance in vehicle supply and demand between different regions or time periods (Nourinejad et al., 2015; Kek et al., 2009; Yang et al., 2021a). To tackle this challenge, operators typically perform relocations. Two main relocation strategies have been proposed and implemented: operator-based and user-based relocations. Operator-based relocations involve hiring staff to move vehicles between stations (Nourinejad et al., 2015; Zhao et al., 2018; Yang et al., 2021a; Chang et al., 2022; Caggiani et al., 2021). On the other hand, the user-based relocation strategy incentivizes users to participate in vehicle repositioning by offering rewards such as discounts or monetary incentives (Jorge et al., 2015; Wang et al., 2021; Zhan et al., 2022; Di Febbraro et al., 2019; Zhang et al., 2022; Stokkink and Geroliminis, 2021). Operator-based relocations are generally more straightforward and easier to implement compared to user-based approaches (Santos and de Almeida Correia, 2019). Accordingly, this paper specifically focuses on the operator-based relocation strategy.

The utilization of EVs presents challenges in managing relocations due to the necessity of monitoring the state of charge (SOC) of the vehicles. Ensuring sufficient remaining battery power for upcoming rentals or relocations is vital to maintaining the operational efficiency of SEV systems. In the current literature, some simplifications are made regarding the recharging process when jointly optimizing recharging and relocation. One common simplification assumes that once vehicles are returned to stations, they are immediately charged and must remain in this charged state for a predetermined duration referred to as “mandatory fixed charge”. Alternatively, they remain charging until fully replenished before being designated for the subsequent trip or relocation, a concept termed “mandatory full charge” (Ait-Ouahmed et al., 2018; Boyacı et al., 2015; Xu et al., 2018; Xu et al., 2020; Brandstätter et al., 2017). Nevertheless, this assumption restricts the utilization of partially charged vehicles especially during peak demand periods. Consequently, this practice could lead to the underutilization of vehicles, an overestimation of the required fleet size, and a reduction in efficiency within carsharing systems. To address this issue, more adaptive and responsive charging strategies are required to optimize energy consumption and enhance infrastructure efficiency. In this context, partial charging has attracted increasing attention, as it allows vehicles to be dispatched with intermediate SOC levels rather than requiring full replenishment.Gambella et al. (2018) and Zhao et al. (2018) adopt space-time network formulations to explicitly model EV charging-related activities, including partial charging processes, alongside user travel, vehicle rebalancing, and staff relocation decisions. Jamshidi et al. (2021) propose a sequential mixed integer linear programming approach to determine the dynamic operations for recharging and relocations of electric taxis. To obtain these executable decisions for individual vehicles, they also adopt the space-time network to track the status of each vehicle. In their directed graph, the daily operational period is divided into a number of small intervals. Each node corresponds to a station during a specific time interval in the space-time network. They meticulously factor in EV battery consumption and the recharging process within their daily operational optimization model. They track the SOC of each vehicle by explicitly defining a time-dependent state variable. However, it is worth noting that the approach adopted by Gambella et al. (2018) and Zhao et al. (2018) involves a comprehensive depiction of the activities of each vehicle. Unfortunately, this level of detail results in complex, large-scale models that prove to be computationally intractable when applied to real-world carsharing systems.

Apart from the space-time network, a comprehensive representation method for vehicle status has gained attention in the literature, known as the space-time-energy network (Santos et al., 2023; Bekli et al., 2021; Zhang et al., 2019; Chen and Liu, 2023; Zhang

et al., 2021). This approach avoids the explicit modeling of individual vehicles by aggregating vehicles with identical battery states. The space-time-energy network flow model serves as an extension of the conventional space-time network flow model. In addition to considering stations and time intervals, this modelling approach discretizes battery capacity into several levels, enabling the monitoring of SOC over time. Each node in the network is represented by a triple: station, time and energy. Zhang et al. (2019) are among the early studies to adopt the space-time-energy network flow model to formulate the EV assignment problem with the decision of EV routing, relocation and charging. Recognizing the uncertainties in demand and the existence of multiple charging outlets, Chen and Liu (2023) expand upon the work of Zhang et al. (2019) by proposing an event-activity space-time-energy network. This enhanced model explicitly captures diverse characteristics of different charging facilities and enables the tracking of charging choices and battery levels of vehicles. Expanding the consideration to various types of charging outlets, Santos et al. (2023) also incorporate different types of vehicles with varying battery capacities and energy consumption rates. They develop the space-time-energy model to determine the movement and charging of EVs, as well as the required number of vehicles and charging facilities.

Using the space-time-energy network flow model avoids the need to individually model each vehicle, thus reducing computational complexity to some extent. Additionally, the model eliminates the need for a restrictive assumption such as the “mandatory full charge”. The replication of each station and battery level based on the number of time intervals provides a direct and intuitive representation of vehicle movement. This approach enables a comprehensive tracking of the overall vehicle status, including their location and battery level. These advantages serve as the primary motivations for adopting the space-time-energy network flow model in formulating the problem addressed in this study.

2.1.2. Integration of vehicle-to-grid with shared electric vehicles

The research on the combination of V2G and SEV is still in its early stages, but its potential and prospects have recently attracted considerable attention. According to a study conducted by Liao et al. (2021), the integration of V2G services into SEV fleets has been examined for its economic and environmental advantages. The study reveals that, on average, each vehicle participating in V2G services could bring an annual revenue of $2,272 while simultaneously reducing greenhouse gas emissions by 66.5 tons per year. To fully unleash the benefits of V2G and SEV integration, optimizing the charging and discharging processes of SEVs has become a crucial operational aspect. Various methodologies have been introduced to address operational problems stemming from the integration of V2G and SEV.

Freund et al. (2012) present one of the earliest studies in introducing the integration of V2G with carsharing. They focus on developing an agent-based control architecture for local energy management in a smart distribution feeder. Their objective is to maximize energy utilization by considering the involvement of various stakeholders, including the smart grid operator, carsharing operator, and distribution system operator. Iacobucci et al. (2019) propose an innovative model that optimizes both transport service and charging at distinct time scales using two model-predictive control optimization algorithms. Longer time scales optimize vehicle charging to minimize electricity costs, while shorter time scales focus on vehicle routing and rebalancing to reduce passenger waiting times.

Recognizing the significance of price sensitivity in influencing user behavior, Ren et al. (2019) propose a dynamic pricing scheme for a large-scale SEV network integrated with V2G. Using predicted station-level travel demand, they formulate the dynamic pricing problem as an optimization model that considers demand-driven electricity pricing, vehicle relocation, and charging and discharging scheduling.

Taking into account uncertainties in carsharing demand and electricity price, Zhang et al. (2021) develop a two-stage stochastic integer programming model to optimize various aspects, including service coverage, EV battery capacity choice, fleet deployment, and parking space capacity. To capture the uncertainties, they consider a range of demand-price scenarios. They construct a space-time-energy network for each scenario, enabling them to dynamically model daily operations involving EV rentals, relocation, idling, charging, and electricity selling to the grid.

Similarly, considering the fluctuation of electricity price, Li et al. (2022) propose a Markov decision model to determine the optimal time allocations for a fleet of SEVs in both the transportation system and the power market to maximize the total profit. An efficient dynamic programming algorithm is adopted to solve the proposed model. Notably, in their work, the EV fleet is regarded as a whole, without considering detailed routes of individual EVs. This simplification could encounter challenges in practical implementation.

Under the assumption that relocation is performed at non-operational hours, Caggiani et al. (2021) propose optimization models to determine the EV distribution among stations at the beginning of each day to maximize profit from V2G operations while meeting the carsharing demand as much as possible.

Similarly, Prencipe et al. (2022) adopt the static relocation approach and propose a mixed integer linear programming model to determine the EV distribution at the beginning of a day and the optimal daily charging/discharging schedules to maximize the revenue from carsharing users and V2G profit. While static relocation simplifies the problem and reduces computational complexity, its lack of responsiveness to dynamic fluctuations in demand may lead to inefficient vehicle utilization.

2.2. Battery swapping

Battery swapping allows users to replace depleted batteries with fully charged ones and has been recognized as an appropriate substitute for conventional fuel stations (Revankar and Kalkhambkar, 2021). Wu (2022) gives a comprehensive review of the current research on the planning and operational challenges in battery swapping systems. The author highlights that the operational scenarios in battery swapping are intricate, necessitating further advancements in optimization methods. Currently, a commonly used mode is the charging-swapping mode, where users can exchange their batteries for fully charged ones at designated battery swapping

stations, and subsequently, their depleted batteries can be recharged at these stations (Shaker et al., 2023). Another mode involves mobile battery swapping, where a battery swapping van delivers fully charged batteries to battery swap demand points and transports depleted ones to battery swapping stations (Yang et al., 2021b). This study focuses specifically on the former station-based swapping mode.

When an EV requests a battery swap, the operator determines an appropriate swapping station, a decision commonly referred to in the literature as the vehicle-to-station assignment problem. You et al. (2018) study this problem and propose an optimization model that assigns the most suitable station for swapping a depleted battery to each EV based on its current location and SOC. The assignment aims to minimize a weighted sum of EVs' travel distance and electricity generation cost. Notably, their approach does not track charging schedules, which leads to each fully charged battery being used to replace depleted batteries at most once. Wang and Hou (2023) study a real-time vehicle-to-station recommendation optimization problem considering EV owners' options. They develop a least-time strategy aiming at minimizing EV owners' time lost. To achieve a globally optimal recommendation, they employ rolling horizon optimization and Lyapunov optimization approaches.

With the involvement of microgrids, battery swapping stations can realize B2G interactions (Revankar and Kalkhambkar, 2021; Cui et al., 2023). Jordehi et al. (2020) propose a nonlinear programming model to determine the optimal power flow at the battery swapping stations taking into account the B2G operation. Results show the economic benefits with the involvement of B2G. Considering the battery condition, swapping/charging demand, and fluctuating electricity prices over time, the operator faces the task of determining an optimal charging/discharging schedule for the batteries. Confronted with the random customer request problem, Mahoor et al. (2019) develop a robust optimization approach to determine the worst-case solution for the optimal battery involving B2G applications. This schedule includes the charging and discharging power of each battery at each time slot, considering the revenue from power sales to the grid, costs of purchasing power, and battery degradation costs. In their model, the state of each battery at each time is tracked with various states. As the number of batteries increases, the complexity of the problem also grows. However, they do not develop specific algorithms to address this challenge. Consequently, there are limitations in the practical application of large-scale problems due to the considerable time consumption required.

2.3. Research gaps and contributions

As previously reviewed, several models and methods have been developed to optimize the recharging process of EVs, but they mostly focus on the plug-in charging. Unfortunately, this recharging method often results in long charging times for EVs, even with fast charging. In contrast, battery swapping offers a promising alternative that enables EVs to be fully recharged in a short period. It has the potential to complement the plug-in charging approach. It is worth noting that while battery swapping holds potential for EV recharging, there is little research conducted on its application within carsharing systems, even though carsharing seems to be a suitable context for such an approach.

Recognizing this research gap, we are motivated to study the integration of battery swapping and plug-in charging within SEV systems. From the previous review, we can observe that the primary concern of models and methods discussed above focusing on the operational management of battery swapping is ensuring that individual vehicles can access the stations and efficiently exchange their batteries based on the vehicle arrival information. However, the applicability of these models and methods to the context of SEVs is not guaranteed. We argue that the integration of battery swapping stations into SEV operations introduces greater complexity. The demand for SEVs and the movement of these vehicles directly influences the operational decisions associated with battery swapping. Therefore, any model or approach aiming to address battery swapping within SEV systems needs to account for this mutual relationship. Surprisingly, to the best of our knowledge, scant research has been conducted in this area, which serves as one of the motivations for this study.

The integration of various technologies associated with the power energy transmission holds the promise of enhancing user satisfaction, boosting vehicle and battery utilization, and unlocking additional benefits (Noel et al., 2019; Liao et al., 2021). While these advantages are well recognized, existing research, as summarized in Table 1, has typically tackled only one or two of these aspects as optimization problems. The inclusion of each additional technology option expands the space of feasible vehicle activity strategies, thereby causing a combinatorial explosion in the problem's complexity. For instance, if a vehicle with SOC of 0% is present at the station which only has plug-in charging available, it cannot immediately serve a user. Instead, it will have to be charged at the station for some time and only later be able to serve other users. When battery swapping is an option, the potential strategies involve the empty-battery vehicle serving a user after a battery swap or the system opting not to serve a user with that vehicle and instead keep the vehicle charging its battery. If V2G technology is present, there is the possibility of the empty-battery vehicle supplying power to the grid following battery swapping due to V2G capabilities. Extending further, a combination of battery swapping, V2G, and B2G provides additional flexibility, as B2G allows a battery at a charging station to supply power to the grid without being installed in a vehicle. As the number of available options increases, decision-making becomes more complex, requiring a careful balance between the costs and revenues associated with each potential strategy. This complexity is a key reason why a comprehensive optimization framework for charging/discharging scheduling, incorporating the amalgamation of plug-in charging, battery swapping, V2G, and B2G, has not been proposed thus far.

To bridge the aforementioned gaps, this study focuses on the optimization of SEV systems in the context of V2G and B2G applications, while also considering the integration of plug-in charging and battery swapping, particularly in real-time operations. The main contributions of this paper are summarized as follows.

(i) Conception and model. Unlike existing studies that focus on a single charging or energy management strategy, this paper considers a coordinated SEV system optimization problem that incorporates multiple energy interaction modes, including battery

Table 1
Summary of previous studies related to the operation of SEVs.

Articles	Recharging modes	Decisions	Modeling and solution methods	V2G/B2G
Xu et al. (2020)	Plug-in charging and mandatory full charge	Charging station deployment	Mixed-integer nonlinear programming model, outer approximation approach	Neither
Ait-Ouahmed et al. (2018)	Plug-in charging and mandatory full charge	Relocation	Mixed integer linear programming, tabu search algorithm	Neither
Boyacı et al. (2015)	Plug-in charging and mandatory fixed charge	Relocation	Multi-objective stochastic programming	Neither
Xu et al. (2018)	Plug-in charging and mandatory full charge	Fleet size, pricing, relocation	Mixed-integer convex programming, outer-approximation algorithm	Neither
Zhao et al. (2018)	Plug-in charging and partial charging	Relocation, allocation, charging scheduling	Space-time network, Lagrangian relaxation-based algorithm	Neither
Bekli et al. (2021)	Plug-in charging and partial charging	Charger location, relocation, assignment	Space-time-energy network, customized heuristic algorithms	Neither
Gambella et al. (2018)	Plug-in charging and partial charging	Relocation, assignment, charging scheduling	Space-time network, customized algorithm	Neither
Huang et al. (2018)	Plug-in charging and partial charging	Fleet size, relocation, charging scheduling	Space-time network, customized algorithm	Neither
Chen and Liu (2023)	Plug-in charging and partial charging	Location, deployment, fleet size, relocation, charging scheduling	Space-time-energy network, two-stage stochastic programming	Neither
Zhang et al. (2019)	Plug-in charging and partial charging	Assignment, relocation, charging scheduling	Space-time-energy network, brand and cut algorithm	Neither
Santos et al. (2023)	Plug-in charging and partial charging	Fleet size, charging facility deployment, relocation, charging scheduling	Space-time-energy network	Neither
Zhang et al. (2021)	Plug-in charging and partial charging	Location, allocation, relocation, charging/discharging scheduling	Space-time-energy network, Benders decomposition	Only V2G
Iacobucci et al. (2019)	Plug-in charging and partial charging	Relocation, charging/discharging scheduling	Model-predictive control optimization algorithm	Only V2G
Li et al. (2022)	Plug-in charging and partial charging	Allocation, charging/discharging scheduling	Markov decision model, dynamic programming algorithm	Only V2G
Yang et al. (2021b)	Battery swapping	Location, routing	Data-driven approach	Neither
This paper	Plug-in charging, partial charging and battery swapping	Relocation, allocation, charging/discharging scheduling	Space-time-energy network, CG-based heuristic algorithm	V2G and B2G

swapping, plug-in charging, and bidirectional energy exchanges such as V2G and B2G. To address this problem, we develop a space-time-energy network-based mathematical model that explicitly captures the coupling between vehicle operations and battery-grid interactions.

(ii) Solution method. We propose a solution framework tailored to large-scale and dynamic decision-making. A CG-based heuristic algorithm is developed to improve computational efficiency, and a rolling horizon approach is incorporated to support real-time decision-making under dynamic demand. Numerical experiments demonstrate that the proposed method yields higher-quality solutions while significantly reducing computational time for large-scale instances, outperforming a commercial solver.

(iii) Managerial insights. The paper delivers managerial guidance for battery-swappable electric carsharing systems by developing and testing a decision-support framework that links charging rates, battery swapping deployment, and energy management strategies. Through numerical experiments, the framework supports infrastructure prioritization under demand and fleet constraints and enables the assessment of V2G and B2G strategies for energy balancing and service performance improvement.

3. Model formulation and small-scale cases

This study proposes an integrated optimization model for the operational decision-making in one-way station-based electric carsharing systems. In such systems, users can pick up and return SEVs at designated stations. Moreover, the system incorporates a combination of charging and discharging technologies, including plug-in charging, battery swapping, V2G and B2G. The proposed model aims to jointly optimize the scheduling of battery and EV charging/discharging, as well as EV relocation and battery swapping operation. Before presenting the mathematical model, the following subsection provides a detailed description of the model's definitions and formulation.

3.1. Definitions and formulation

Time. The operational timeframe is denoted by T and is divided into a set of time intervals with uniform durations, denoted as $\{1, 2, \dots, t, \dots, |T|\}$, where 1 and $|T|$ denote the start and end of the operational period, respectively.

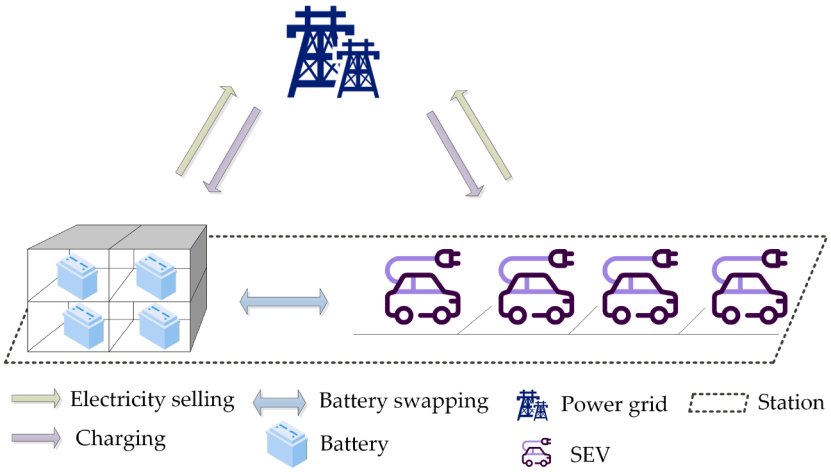


Fig. 1. Illustration of a Type 2 station.

Stations. Stations serve as designated locations where vehicles are picked up and returned, denoted as $I = \{1, 2, \dots, i \dots, |I|\}$. Each station is equipped with a specific number of parking spaces. Depending on the available charging and discharging infrastructure, we consider two types of stations:

- *Type 1*: Stations with only parking spaces but no other infrastructure, denoted by the set $I^{[1]}$.
- *Type 2*: Stations with parking spaces featuring plug-in charging, battery swapping, as well as V2G and B2G infrastructure, denoted by the set $I^{[2]}$. Fig. 1 illustrates the infrastructure layout of a Type 2 station. It is assumed that each parking space in Type 2 stations is outfitted with a charging outlet. Throughout this paper, we assume that the carsharing operator installs and operates its own charging and discharging infrastructure, which is homogeneous across all Type 2 stations.

Vehicles. A fixed homogeneous fleet of SEVs provides carsharing service. The initial vehicle allocation is known. Within this system, SEVs can execute a range of operations, outlined as follows:

- *Rental*: Users rent vehicles for one-way trips. Upon receiving a user request, the carsharing operator needs to determine whether the request can be accepted.
- *Relocation*: Due to the demand imbalance, vehicles could accumulate or become scarce at specific stations. Relocation is employed to rebalance the vehicle distribution. In this study, we consider operator-based relocations, assuming the availability of sufficient staff for performing the relocations. The operator needs to determine the relocation tasks, including when and where vehicle relocations should take place during the operational period.
- *Charging*: Vehicles can be charged at Type 2 stations, with partial charging allowed, meaning they do not need to be fully charged before their next use. The operator must determine the optimal timing, location, and duration for vehicle charging.
- *Energy selling*: Beyond serving carsharing users, vehicles can contribute to the grid network by supplying electricity. The operator needs to decide when, where, and for what duration vehicles should sell electricity to the grid using V2G technology.
- *Battery swapping*: Battery swapping involves replacing a vehicle's depleted battery with a fully charged one at dedicated stations. This operation incurs a non-negligible time cost. In this study, we assume that each battery swapping operation takes one time interval to complete. The operator should decide the appropriate timing, location, and number of vehicles for battery swapping operations.
- *Idle*: Vehicles are parked at stations, not in use or actively participating in any of the tasks mentioned above. These vehicles are awaiting assignment.

Charging and discharging. Battery charging rate mostly depends on both grid condition and the battery's electrochemical properties. Specifically, charging rate varies with SOC, as higher SOC levels typically lead to lower charging rates due to inherent battery characteristics (Xu and Meng, 2019). Additionally, grid voltage fluctuations at different stations over time lead to variations in the available charging power across stations. Therefore, in this paper, we introduce a charging rate parameter (to be detailed later) that varies with both time and SOC at each station to capture these dynamics.

Energy consumption during driving is affected by multiple factors, including vehicle speed, acceleration, ambient temperature, and road gradient, making the precise modeling of energy consumption challenging. For simplicity, we assume that EVs travel at a speed without much variation such that the SOC would decline linearly with travel time (Chen and Liu, 2023; Xu and Meng, 2019). Consequently, we adopt a constant discharge rate per unit time interval. This approximation is reasonable, as supported by Pelletier et al. (2017), whose findings demonstrate that the battery's discharge profile remains approximately linear when an EV travels at a steady speed.

Electricity price. The electricity price for charging and selling is the same at any given time, but it fluctuates throughout the day.

Batteries. In this study, batteries owned by operators are uniform and can be classified into two types: *vehicle-installed* and *stocked* (Wang et al., 2019). Stocked batteries are physically kept in dedicated charging boxes at Type 2 stations and come with four

statuses: idle, charging, energy selling, and swapping (You et al., 2018). This means that a battery is either installed in a vehicle or stored at a Type 2 station. When the vehicle-installed batteries are nearing depletion, EVs can move to Type 2 stations to swap their empty batteries with the fully-charged stocked ones. When a vehicle-installed battery is swapped out to be stored at a station, simultaneously, another stocked battery is swapped in to become vehicle-installed. This exchange ensures that the total number of stocked batteries at each Type 2 station remains constant over time. At the start of operation hours, the initial allocation and SOC of each battery are known. Our study addresses the following statuses concerning stocked batteries:

- *Charging*: The charging rate of a battery in a charging box is the same as when it is installed in a vehicle.
- *Energy selling*: With B2G technology, stocked batteries have the capability to directly feed electricity into the grid without relying on electric vehicles. The operator should decide when stocked batteries should sell electricity, taking into account factors such as EV usage demand and electricity prices.
- *Swapping*: Fully charged stocked batteries can be used to replace depleted vehicle-installed batteries.
- *Idle*: In this status, stocked batteries are not engaged in charging, energy selling, or swapping activities. They are temporarily unassigned to specific tasks, simply stored at the Type 2 station, awaiting future operations.

Vehicle-installed batteries are installed within vehicles, with their statuses aligned with vehicle operations. Since vehicle statuses have been previously detailed, all subsequent discussions of battery statuses in this paper specifically refer to stocked batteries unless otherwise stated.

Demand. User requests consist of trip information, including origin, destination, and trip starting time. Demand represents a collection of requests that share common trip characteristics. Regarding the reservation rule of instant reservation systems, we follow the setting adopted by Nourinejad and Roorda (2014), Yang et al. (2021a) and Liang et al. (2020), which incorporates a reservation period between request submission and actual pickup time.

3.2. A space-time-energy network-based optimization model

A flow-based integer programming model is built on a three-dimensional space-time-energy network, which extends the conventional space-time network flow model by incorporating SOC level information. Each node in the network represents a specific combination of location, time, and SOC level. SOC levels are discretized into a set of percentage-based intervals, denoted by E. Let $n_{i,t,e}$ denote a node representing either a vehicle or a stocked battery with SOC level $e \in E$, located at station i at time t. For the sake of model formulation, virtual source nodes are introduced, represented as $n_{i,0,e}$. Here, 0 serves as the dummy time interval. Arcs between nodes represent the activities of vehicles and stocked batteries. Depending on the operations of vehicles and stocked batteries, these arcs can be categorized into the following sets:

Rental arcs of vehicles: $\left(n_{i,t,e}, n_{j,k,r}\right) \in A^{\text{rent}}$ for $i, j \in I$, $t, k \in T$, and $e, r \in E$, connecting node $n_{i,t,e}$ to $n_{j,k,r}$. Flow on the arc represents the number of SEVs with SOC level e which are rented by users to travel from station i to j starting at the beginning of time interval t. The arrival time interval at station j is calculated by $k = t + \tau_{i,j}$, and the remaining SOC upon arrival is given by $r = e - \beta^{\text{D}}\tau_{i,j}$, where $\tau_{i,j}$ is the travel time from station i to station j, measured in time intervals, and β^{D} is the discharging rate per unit time interval. For operators, the revenue generated from each unit flow on rental arc $\left(n_{i,t,e}, n_{j,k,r}\right)$ is computed by $p^{\text{rental}}\tau_{i,j}$, where p^{rental} is the rental fee per time interval for one SEV.

Relocation arcs of vehicles: $\left(n_{i,t,e}, n_{j,k,r}\right) \in A^{\text{relo}}$ for $i, j \in I$, $t, k \in T$, and $e, r \in E$, connecting node $n_{i,t,e}$ to $n_{j,k,r}$. Flow on the arc represents the number of SEVs with SOC level e which are relocated by staff to travel from station i to j starting at time interval t. The arrival time interval at station j is calculated by $k = t + \tau_{i,j}$, and the remaining SOC level upon arrival is given by $r = e - \beta^{\text{D}}\tau_{i,j}$. For operators, the unit flow cost on the relocation arc $\left(n_{i,t,e}, n_{j,k,r}\right)$ is $c^{\text{relo}}_{i,j}$.

In this paper, we assume that vehicles travel directly from the origin station to the destination station along the shortest available route, without intermediate stops. Accordingly, $\tau_{i,j}$ is calculated as the shortest travel time along the road network connecting the two stations, using standard shortest-path algorithms, such as Dijkstra's algorithm. From the operator's perspective, vehicle relocations aim to maximize fleet utilization and service efficiency. Assigning vehicles along the shortest paths helps reduce energy consumption and improve vehicle turnover, and is therefore consistent with the operator's efficiency-oriented objectives. In addition, this study does not explicitly model individual users' route choices or stochastic variations in travel time. Consequently, the shortest travel time is used to approximate rental travel time, as is commonly adopted in network-flow models of station-based carsharing systems.

Idle arcs of vehicles: $\left(n_{i,t,e}, n_{i,t+1,e}\right) \in A^{\text{idle}}$ for $i \in I$, $t \in T^{[1]}$, and $e \in E$, connecting node $n_{i,t,e}$ to $n_{i,t+1,e}$, where $T^{[1]} = \{1, \ldots, |T| - 1\} \subset T$. Flow on the arc represents the number of SEVs with SOC level e remaining idle at station i from time interval t to $t + 1$. In this case, these vehicles do not change either in space or energy but only advance in time.

Charging arcs of vehicles: $\left(n_{i,t,e}, n_{i,t+1,r}\right) \in A^{\text{charg}}$ for $i \in I^{[2]}$, $t \in T^{[1]}$, and $e, r \in E(e < |E|)$, connecting node $n_{i,t,e}$ to $n_{i,t+1,r}$. Flow on the arc represents the number of SEVs undergoing charging at station i from time interval t to $t + 1$, where the SOC level of SEVs is updated from e to r. The SOC level update is given by $r = \min(e + \beta^{\text{C}}_{i,t,e}, |E|)$, where $\beta^{\text{C}}_{i,t,e}$ denotes the charging rate at station i during time interval t for SEVs or stocked batteries with SOC level e. For operators, the unit flow cost on charging arc $\left(n_{i,t,e}, n_{i,t+1,r}\right)$ is $Q(r - e)p^{\text{ele}}_t$, where Q is the maximum capacity of a battery, expressed in kWh, and p^{ele}_t is the electricity price at time interval t. It should be noted that the electricity prices are exogenously determined by the utility provider and are not controlled by the carsharing operator. The operator is responsible for installing and managing the charging/discharging infrastructure for its own fleet. Since this study focuses on operational decisions under a pre-existing and homogeneous infrastructure, differences in charging costs across facilities are not considered.

Energy selling arcs of vehicles: $\left(n_{i,t,e}, n_{i,t+1,r}\right) \in A^{\text{sell}}$ for $i \in I^{[2]}$, $t \in T^{[1]}$, and $e, r \in E(e > 0)$, connecting node $n_{i,t,e}$ to $n_{i,t+1,r}$. Flow on the arc represents the number of SEVs selling electricity back to the grid at station i from time interval t to $t + 1$ and the SOC

decreasing from e to r, where the updated SOC level r is given by $r = \max(0, e - \beta^{\mathrm{D}})$. For operators, the revenue generated from each unit flow on the energy selling arc $\left(n_{i,t,e}, n_{i,t+1,r}\right)$ is $Q(e-r)p_t^{\mathrm{ele}}$.

Battery swapping arcs of vehicles: $\left(n_{i,t,0}, n_{i,t+1,|E|}\right) \in A^{\mathrm{swap}}$ for $i \in I^{[2]}$ and $t \in T^{[1]}$, connecting node $n_{i,t,0}$ to $n_{i,t+1,|E|}$. Flow on the arc represents the number of SEVs with depleted batteries swapping batteries at station i from time interval t to $t+1$. After the swap, the vehicle's battery state is reset to full charge. For operators, the unit flow cost on a battery swapping arc is c^{swap}.

Idle arcs of stocked batteries: $\left(n_{i,t,e}, n_{i,t+1,e}\right) \in B^{\mathrm{idle}}$ for $i \in I^{[2]}$, $t \in T^{[1]}$, and $e \in E$, connecting node $n_{i,t,e}$ to $n_{i,t+1,e}$. Flow on the arc represents the number of stocked batteries with SOC level e idling at station i from time interval t to $t+1$.

Charging arcs of stocked batteries: $\left(n_{i,t,e}, n_{i,t+1,r}\right) \in B^{\mathrm{charg}}$ for $i \in I^{[2]}$, $t \in T^{[1]}$, and $e, r \in E(e < |E|)$, connecting node $n_{i,t,e}$ to $n_{i,t+1,r}$. Flow on the arc represents the number of stocked batteries being charged at station i from time interval t to $t+1$, where SOC level is updated from e to r. The SOC level update is given by $r = \min(e + \beta_{i,t,e}^{\mathrm{C}}, |E|)$. For operators, the cost per unit flow on charging arc $\left(n_{i,t,e}, n_{i,t+1,r}\right)$ is $Q(r-e)p_t^{\mathrm{ele}}$.

Energy selling arcs of stocked batteries: $\left(n_{i,t,e}, n_{i,t+1,r}\right) \in B^{\mathrm{sell}}$ for $i \in I^{[2]}$, $t \in T^{[1]}$, and $e, r \in E(e > 0)$, connecting node $n_{i,t,e}$ to $n_{i,t+1,r}$. Flow on the arc represents the number of stocked batteries selling electricity back to the grid at station i from time interval t to $t+1$ with SOC level decreasing from e to r, where the updated SOC level r is given by $r = \max(0, e - \beta^{\mathrm{D}})$. For operators, the revenue generated from each unit flow on the energy selling arc $\left(n_{i,t,e}, n_{i,t+1,r}\right)$ is $Q(e-r)p_t^{\mathrm{ele}}$.

Battery swapping arcs of stocked batteries: $\left(n_{i,t,|E|}, n_{i,t+1,0}\right) \in B^{\mathrm{swap}}$ for $i \in I^{[2]}$ and $t \in T^{[1]}$, connecting node $n_{i,t+1,|E|}$ to $n_{i,t,0}$. Flow on the arc represents the number of stocked fully-charged batteries being exchanged with depleted vehicle-installed batteries at station i from time interval t to $t+1$.

Dummy source arcs: For vehicles, the dummy source arc is $\left(n_{i,0,e}, n_{i,1,e}\right) \in A^{\mathrm{source}}$ for $i \in I$ and $e \in E$, and flow on the arc represents the number of SEVs with SOC level e initially located at station i. For stocked batteries, the dummy source arc is $\left(n_{i,0,e}, n_{i,1,e}\right) \in B^{\mathrm{source}}$ for $i \in I^{[2]}$ and $e \in E$, and flow on the arc represents the number of stocked batteries with SOC level e initially stored at station i.

The notations used in our formulation are summarized in Table 2.

The integrated optimization framework for the scheduling of SEVs and stocked batteries is formulated as a space-time-energy network flow model, denoted as [P]. The objective and constraints of this model are as follows.

$$\max \quad \sum_{a \in A^{\mathrm{rent}} \cup A^{\mathrm{sell}}} p_a x_a + \sum_{b \in B^{\mathrm{sell}}} p_b y_b - \sum_{a \in A^{\mathrm{relo}} \cup A^{\mathrm{charg}}} c_a x_a - \sum_{b \in B^{\mathrm{charg}} \cup B^{\mathrm{swap}}} c_b y_b \tag{1}$$

$$\text{s.t.} \quad \sum_{a=(n_{i,0,e}, n_{i,1,e}) \in A^{\mathrm{source}}} x_a = \lambda_{i,0,e}^{\mathrm{V}}, \quad \forall i \in I,\ e \in E \tag{2}$$

$$\sum_{a \in \zeta_{i,t,e}^{+}} x_a - \sum_{a \in \zeta_{i,t,e}^{-}} x_a = 0, \quad \forall i \in I,\ t \in T^{[1]},\ e \in E \tag{3}$$

$$\sum_{a \in A_{i,j,t}^{\mathrm{rent}}} x_a \le d_{i,j,t}, \quad \forall i, j \in I,\ t \in T \tag{4}$$

$$\sum_{a \in \zeta_{i,t,e}^{-} \cap A^{\mathrm{rent}}} x_a \le \sum_{a \in \zeta_{i,t,e}^{+} \cap A^{\mathrm{idle}}} x_a, \quad \forall i \in I,\ t \in T,\ e \in E \tag{5}$$

$$\sum_{a \in A_{i,t}^{\mathrm{start}} \cap A^{\mathrm{park}}} x_a \le m_i, \quad \forall i \in I,\ t \in T \tag{6}$$

$$\sum_{b=(n_{i,0,e}, n_{i,1,e}) \in B^{\mathrm{source}}} y_b = \lambda_{i,0,e}^{\mathrm{B}}, \quad \forall i \in I^{[2]},\ e \in E \tag{7}$$

$$\sum_{b \in \theta_{i,t,e}^{+}} y_b - \sum_{b \in \theta_{i,t,e}^{-}} y_b = 0, \quad \forall i \in I^{[2]},\ t \in T^{[1]},\ e \in E \tag{8}$$

$$\sum_{a \in \zeta_{i,t,0}^{-} \cap A^{\mathrm{swap}}} x_a = \sum_{b \in \theta_{i,t,|E|}^{-} \cap B^{\mathrm{swap}}} y_b, \quad \forall i \in I^{[2]},\ t \in T^{[1]} \tag{9}$$

$$x_a, y_b \in \mathbb{Z}_{\ge 0}, \quad \forall a \in A,\ b \in B \tag{10}$$

Objective function (1) maximizes the overall profit, which is formulated as the difference between total revenues and total costs. Revenues arise from fulfilled user requests and the sale of electricity from both SEVs and stocked batteries, whereas costs consist of the relocation costs, electricity buying costs, and battery swapping costs. Fixed costs, such as vehicle and battery depreciation, are excluded from the objective function, as they are considered exogenous parameters in this study and do not affect the optimization results.

Constraint (2) specifies the initial distribution of vehicles by mapping the number of vehicles with SOC level e initially located at station i to the flow on dummy source arc $\left(n_{i,0,e}, n_{i,1,e}\right)$. Constraints (3) represent the flow conservation constraints at space-time-energy nodes. Constraints (4) require that the number of SEVs assigned to trip requests with origin i, destination j and departure time t should not exceed the demand for the origin-destination (OD) pair. Constraints (5) ensure that a sufficient number of idle vehicles are available to serve trips departing from station i at time interval t. Constraints (6) ensure that the number of vehicles parked at station i at the beginning of a given time interval cannot exceed the capacity of the station. It should be noted that for station $i \in I^{[1]}$, the parked vehicles include idle vehicles; for station $i \in I^{[2]}$, the parked vehicles include idle vehicles, vehicles being charged, vehicles selling electricity, and vehicles that are swapping their batteries.

Table 2
Notations for the model formulation.

Sets and indices	Description
I	Set of stations, $I = \{1, \dots, \lvert I \rvert\}$ indexed by i and j
$I^{[1]}$	Set of Type 1 stations, which solely used for parking without recharging infrastructure
$I^{[2]}$	Set of Type 2 stations with infrastructure supporting plug-in charging, battery swapping, V2G and B2G
T	Set of time intervals, $T = \{1, \dots, \lvert T \rvert\}$, indexed by t and k
$T^{[1]}$	Set of time intervals, $T^{[1]} = \{1, \dots, \lvert T \rvert - 1\} \subset T$
E	Set of SOC levels, $E = \{0, \dots, \lvert E \rvert\}$, indexed by e and r
A^{rent}	Set of vehicle rental arcs in the space-time-energy network
A^{relo}	Set of vehicle relocation arcs in the space-time-energy network
A^{idle}	Set of vehicle idle arcs in the space-time-energy network
A^{charg}	Set of vehicle charging arcs in the space-time-energy network
A^{sell}	Set of vehicle energy selling arcs in the space-time-energy network
A^{swap}	Set of swapping batteries arcs of vehicles in the space-time-energy network
A^{source}	Set of vehicle source arcs in the space-time-energy network
A	Set of vehicle arcs, $A = A^{\text{rent}} \cup A^{\text{relo}} \cup A^{\text{idle}} \cup A^{\text{charg}} \cup A^{\text{sell}} \cup A^{\text{swap}} \cup A^{\text{source}}$, indexed by a
A^{park}	A subset of A, $A^{\text{park}} = A^{\text{idle}} \cup A^{\text{charg}} \cup A^{\text{sell}} \cup A^{\text{swap}}$
B^{idle}	Set of stocked battery idle arcs in the space-time-energy network
B^{charg}	Set of stocked battery charging arcs in the space-time-energy network
B^{sell}	Set of stocked battery energy selling arcs in the space-time-energy network
B^{swap}	Set of stocked battery swapping arcs in the space-time-energy network
B^{source}	Set of stocked battery source arcs in the space-time-energy network
B	Sets of stocked battery arcs, $B = B^{\text{idle}} \cup B^{\text{charg}} \cup B^{\text{sell}} \cup B^{\text{swap}} \cup B^{\text{source}}$, indexed by b
$\zeta^{-}_{i,t,e}$	Set of arcs for which node $n_{i,t,e}$ ($i \in I$, $t \in T$, and $e \in E$) is the origin node of SEVs
$\zeta^{+}_{i,t,e}$	Set of arcs for which node $n_{i,t,e}$ ($i \in I$, $t \in T$, and $e \in E$) is the destination node of SEVs
$\theta^{-}_{i,t,e}$	Set of arcs for which node $n_{i,t,e}$ ($i \in I^{[2]}$, $t \in T$, and $e \in E$) is the origin node of stocked batteries
$\theta^{+}_{i,t,e}$	Set of arcs for which node $n_{i,t,e}$ ($i \in I^{[2]}$, $t \in T$, and $e \in E$) is the destination node of stocked batteries
$A^{\text{start}}_{i,t}$	A subset of A, arcs originating from station $i \in I$ starting from time interval $t \in T$, $A^{\text{start}}_{i,t} = \left\{ \left(n_{i,t,e}, n_{j,k,r} \right) \in A \mid j \in I, k \in T, e, r \in E \right\}$
$A^{\text{rent}}_{i,j,t}$	A subset of A^{rent}, rental arcs from station $i \in I$ to $j \in I$ starting from time interval $t \in T$, $A^{\text{rent}}_{i,j,t} = \left\{ (n_{i,t,e}, n_{j,k,r}) \in A^{\text{rent}} \mid e, r \in E \right\}$
Parameters	**Description**
p^{rental}	Revenue from a SEV per time interval when rented by a user
p^{ele}_{t}	Unit electricity prices of charging or selling during time interval $t \in T$
$c^{\text{relo}}_{i,j}$	Cost of relocating a SEV from station $i \in I$ to $j \in I$
c^{swap}	Cost of swapping a battery
p_a	Revenue from vehicle arc $a \in A$
p_b	Revenue from battery arc $b \in B$
c_a	Cost of vehicle arc $a \in A$
c_b	Cost of battery arc $b \in B$
Q	Maximum capacity of a battery, expressed in kWh
$\tau_{i,j}$	Travel time from station $i \in I$ to $j \in I$
m_i	Number of parking spaces at station $i \in I$
$\lambda^{\text{V}}_{i,0,e}$	Initial number of vehicles with SOC level $e \in E$ parked at station $i \in I$
$\lambda^{\text{B}}_{i,0,e}$	Number of stoked batteries with initial SOC level $e \in E$ stored at station $i \in I^{[2]}$
$\beta^{\text{C}}_{i,t,e}$	Charging rate at station $i \in I^{[2]}$ for SEVs or stocked batteries with SOC level $e \in E$ during time interval $t \in T$, in percentage
β^{D}	Discharging rate per unit time interval, in percentage
Decision variables	**Description**
x_a	Integer variables, flow of vehicles on arc $a \in A$
y_b	Integer variables, flow of vehicles on arc $b \in B$

Constraint (7) specifies the initial distribution of stocked batteries by mapping the number of stocked batteries with initial SOC level e stored at station i to the flow on dummy source arc $\left(n_{i,0,e}, n_{i,1,e}\right)$. Constraints (8) ensure the flow conservation for stocked batteries. Constraints (9) indicate that the battery swapping process involves two simultaneous actions. For SEVs, an empty vehicle-installed battery is removed, while a stocked battery comes. For batteries, an empty inside-vehicle battery transforms into a stocked one, while a fully charged battery becomes an inside-vehicle one. Constraints (10) enforce that decision variables x_a and y_b take non-negative integer values.

3.3. Small-scale illustration

We design a small-scale network to demonstrate the output of the proposed model, the test network has the following characteristics: there are 4 stations, 12 time intervals, 3 SEVs, and 10 requests. Stations 1 and 2 are categorized as Type 1, and the remaining two belong to Type 2. SOC levels are discretized into the following levels: {0%, 10%, 20%, 30%, 40%, 50%, 60%, 70%, 80%, 90%, 100%}. Initially, two fully charged vehicles are parked at Station 1, and one vehicle with SOC level of 80% is parked at Station 2. Additionally, Station 3 is equipped with a stocked battery with 40% SOC level, and a fully charged stocked battery is stored at Station 4. For simplicity, the charging rate is set to be constant across all stations, SOC levels, and time intervals, increasing the SOC level

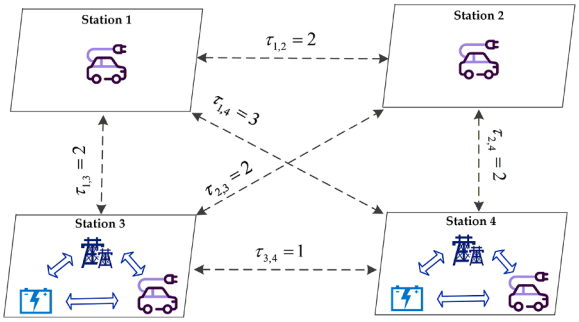


Fig. 2. Travel times between stations (in number of time intervals).

Table 3
Trip demand information.

Origin	Destination	Departure time interval	Quantity
1	2	1	1
2	3	3	1
4	1	7	1
1	4	1	1
4	3	5	2
3	1	7	2
1	3	4	1
1	3	5	1

Table 4
Number of decision variables.

Decision variables	Number of decision variables
x_a	$2\|I\|^2\|T\|\|E\| + \|I\|\|T\|\|E\| + 2\|I^{[2]}\|\|T\|\|E\| + \|I\|\|T\| + \|I\|\|E\|$
y_b	$2\|I^{[2]}\|\|T\|\|E\| + 2\|I^{[2]}\|\|T\| + \|I^{[2]}\|\|E\|$

by 40% per time interval, while the discharging rate remains fixed at 20% per time interval. The electricity price peaks during time intervals 3-4 and 10-11. The travel times between stations are illustrated in Fig. 2, and it should be noted that the travel time is symmetric. Trip demand information including the origin, destination, departure time, and quantity is shown in Table 3.

The solution of the test instance is depicted in Fig. 3. In this figure, the x-axis represents time, the y-axis represents the station index, the z-axis represents SOC levels, and each space-time-energy node is denoted by a grey circle. Colored arrows represent arcs, while the numbers on the arcs represent the flow on the arcs. Fig. 3a illustrates the SEV flows, while Fig. 3b shows the battery flows. As depicted in Fig. 3a, eight out of ten trip requests are fulfilled. The yellow arrow indicates two vehicle relocations: a vehicle moves from Station 2 to Station 1 starting at time interval 1, with its SOC level moves from 80% to 40%; another one relocates from Station 3 to Station 4 beginning at time interval 5, depleting its SOC level from 20% to 0%. Additionally, as shown by the black arrows, one vehicle sells electricity from time interval 4 to 5. To serve more trip demand, a battery swapping operation is conducted at Station 4 from time interval 6 to 7, as depicted by the blue arrow.

As shown in Fig. 3b, both batteries participate in electricity sales during peak-price periods, which are indicated by black dashed arrows. One battery remains idle except for two discharging intervals. Specifically, during time interval 6-7, a fully charged battery is installed in a vehicle, replacing a depleted battery with a SOC of 0%. The battery then remains idle until time interval 9-10, when it is recharged, and subsequently discharges electricity to the grid until the end.

The small-scale example presented here serves solely to illustrate how the system we are modeling looks like. Rigorous validation of the scalability and performance across diverse scenarios will be presented in Section 5.

4. Solution approach

4.1. Computational complexity and model preprocessing

With an extra dimension for tracking battery levels, the state space of the proposed network flow model can expand significantly as the problem scale grows larger. Furthermore, the considered problem is integrated, as it involves the interconnection of vehicle flows and battery flows. Table 4 summarizes the number of decision variables for the mathematical model [P], enabling an analysis of the model complexity. Here, $|\cdot|$ denotes the cardinality of set $\{\cdot\}$.

In the network model, the number of decision variables is determined by the number of arcs. To reduce the problem size, we conduct preprocessing to only consider the necessary arcs and nodes. Among the various sets of arc types, rental arcs and relocation

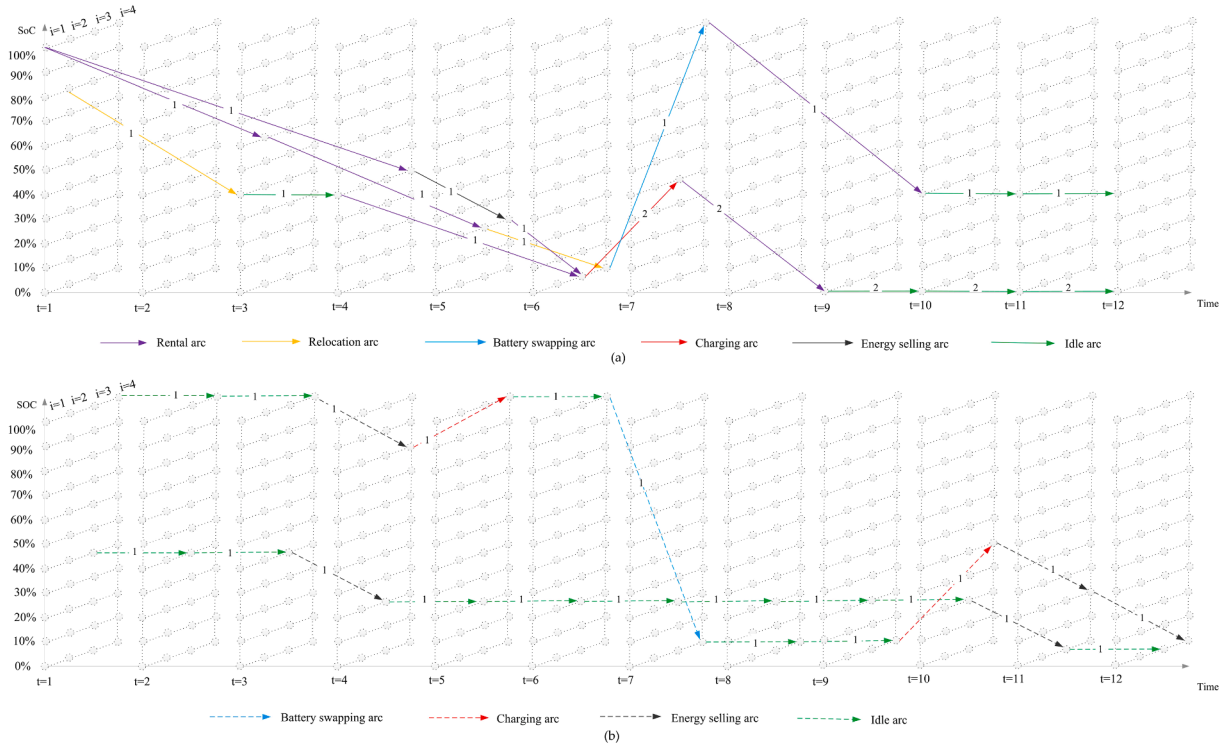


Fig. 3. Flow results of the illustration case.

arcs have the largest number of arcs, with a number of $2|I|^2|T||E|$, which makes it time-consuming to obtain a solution. Hence, it becomes imperative to preprocess them to generate the minimum number of arcs while preserving essential connectivity.

To minimize the number of rental arcs, we generate rental arcs $A^{\text{rent}}_{i,j,t}$ only if a user request exists from station i to j at time t. If there is no demand from station i to j at time t, then $A^{\text{rent}}_{i,j,t}$ is set to be empty. Regarding the relocation arcs, we adopt the approach introduced in Chen and Liu (2023) of identifying hub stations to reduce the number of relocation arcs. For the relocation trip between station i and j, we seek a hub h where the travel time adheres to the condition $\tau_{i,j} = \tau_{i,h} + \tau_{h,j}$. If such a hub h exists, the relocation arcs between station i and j can be eliminated. This is because the relocation trip from station i to j can be completed by using two separate relocation trips: one from station i to h and another from station h to j.

Our preprocessing steps only remove redundant arcs, ensuring no optimal solutions are eliminated. Regarding other types of arcs, no preprocessing is applied. This is because these arcs account for a relatively small proportion of the total arc set, and to our knowledge, there is no effective strategy to significantly reduce them without risking the loss of feasible solutions.

4.2. Column generation-based heuristic algorithm

4.2.1. Reformulation

As introduced, this study considers four activities of stocked batteries: idle, charging, energy selling, and battery swapping. At Type 2 stations, each stocked battery is placed in a charging box. When a depleted inside-vehicle battery is swapped with a fully charged stocked battery, the depleted battery will be deposited in the same box that previously held the fully charged one. This setting indicates that if a charging box contains a battery at the start of the operational timeframe, it will always hold a battery thereafter, though the specific battery and its status may change over time. Under this framework, we define the status of a charging box to align with the activity of the battery currently placed inside it. Accordingly, the status of each charging box can also be classified into four categories: idle, charging, energy selling, and battery swapping. Based on this, we make the following observation:

Observation 1: By tracking the status of charging boxes over time intervals, the flow of stocked batteries is obtained.

To illustrate the relationship between the status of charging boxes and the flow of stocked batteries, we take the idle status arcs as an example for simplification. Following the process of arc construction for batteries, we define idle status arcs $\left(n_{i',t,e}, n_{i',t+1,e}\right) \in B^{\text{idle}}_{\text{box}}$ for box $i' \in I^{\text{box}}$, which means that there is an idle stocked battery with SOC level e placed in box i' from time interval t to $t+1$, where I^{box} is the set of boxes. Subsequently, we introduce a binary variable $\upsilon_{b'}(b' = \left(n_{i',t,e}, n_{i',t+1,e}\right) \in B^{\text{idle}}_{\text{box}})$, which takes the value 1 if there is an idle stocked battery on arc b', and 0 otherwise. Then, the stocked battery flow y_b on the arc $b = \left(n_{i,t,e}, n_{i,t+1,e}\right) \in B^{\text{idle}}$ can be expressed as $y_b = \sum_{b'} \upsilon_{b'}(b' \in \left\{\left(n_{i',t,e}, n_{i',t+1,e}\right) \in B^{\text{idle}}_{\text{box}} | i' \in I^{\text{box}}_i\right\})$, where I^{box}_i is the set of boxes at the station $i \in I$[2]. This equation indicates that the flow of idle stocked batteries at station i is the cumulative sum of boxes belonging to station i that contain idle

stocked batteries during the given time interval. By extending this logic, various other types of stocked battery flows can also be represented using the corresponding status arcs associated with each box. This aligns with the statement made in Observation 1, where by tracking the status of boxes during each time interval, the flow of stocked batteries is obtained.

Based on Observation 1, Constraints (7)–(9) can be replaced with the following constraints:

$$\sum_{b' \in \{(n_{i',0,e}, n_{i',1,e}) \in B^{\text{source}}_{\text{box}} | i' \in I_i^{\text{box}}\}} v_{b'} = \lambda^{\text{B}}_{i,0,e}, \quad \forall i \in I^{[2]}, e \in E \tag{11}$$

$$\sum_{b' \in \vartheta^{+}_{i',t,e}} v_{b'} - \sum_{b' \in \vartheta^{-}_{i',t,e}} v_{b'} = 0, \quad \forall i' \in I^{\text{box}}, t \in T^{[1]}, e \in E \tag{12}$$

$$\sum_{a \in \zeta^{-}_{i,t,0} \cap A^{\text{swap}}} x_a = \sum_{b' \in \bigcup_{i' \in I_i^{\text{box}}} \vartheta^{-}_{i,t,|E|} \cap B^{\text{swap}}_{\text{box}}} v_{b'}, \quad \forall i \in I^{[2]}, t \in T \tag{13}$$

$$v_{b'} \in \{0,1\}, \quad \forall b' \in B^{\text{box}} \tag{14}$$

where I^{box} is the set of all boxes, B^{box} is the set of all state arcs of boxes, and $B^{\text{source}}_{\text{box}}$ is the dummy source arcs of boxes. $\vartheta^{+}_{i',t,e}$ and $\vartheta^{-}_{i',t,e}$ are a set of arcs for which $n_{i',t,e}$ is the destination and origin node, respectively. $B^{\text{swap}}_{\text{box}}$ is the set of swapping arcs of boxes, $B^{\text{swap}}_{\text{box}} = \left\{(n_{i',t,|E|}, n_{i',t+1,0}) | i' \in I^{\text{box}}, t \in T^{[1]}\right\}$. Other notations correspond to those introduced in Section 3.2. By simply substituting the station index in the stocked battery arcs with the box index, all box status arcs can be generated. Hence, the detailed enumeration of these box status arcs is not provided here. Constraints (11)–(13) are equivalent of Constraints (7)–(9), respectively, but written in terms of the variable $v_{b'}$ instead of y_b.

Compared to the formulation in Section 3.2, the above reformulation leads to heightened computational complexity due to the increased number of decision variables. The total number of decision variables has now increased by $\left(2\left|I^{[2]}\right||T||E| + 2\left|I^{[2]}\right||T| + \left|I^{[2]}\right|\right)\left(\sum_{i \in I^{[2]}} \lambda^{\text{B}}_{i,0,e} - 1\right)$. However, this reformulation has an advantage, it is expected to yield solutions by using CG algorithm. In the next subsections, we explain how to apply the CG algorithm to our proposed model.

4.2.2. Master problem

CG is a specialized technique that aims to address large-scale optimization problems. This approach has demonstrated in successful applications in diverse areas such as routing problems (Wang et al., 2023; He et al., 2023), scheduling problems (Zhou et al., 2022;Wu et al., 2022), and more. The fundamental concept of CG is to iteratively solve a master linear programming model and a pricing problem. The master linear programming model includes a subset of variables of the original problem, and it passes dual variables to the pricing problem to find promising columns with negative reduced costs for minimization problems (or positive reduced costs for maximization problems). Subsequently, the decision variables that correspond to these promising columns are incorporated into the master linear programming model. This iterative approach continues until no promising columns can be generated.

For any given box, a sequence of its status arcs within the considered horizon can be represented as a **chain**. This chain consists of a series of status arcs in an ascending order in terms of time. Suppose that the power of the battery inside the box remains at 100% from time interval $t = 1$ to $t = 2$, then sells energy with SOC changing from 100% to 60% during time interval $t = 2$ to $t = 3$, subsequently is charged with SOC returning from 60% to 100% during time interval $t = 3$ to $t = 4$, and finally is swapped with SOC dropping from 100% to 0% during time interval $t = 4$ to $t = 5$. The chain representation for this box i' across these time intervals is as follows: $(i',1,100\%,i',2,100\%)_{\text{idle}} \Rightarrow (i',2,100\%,i',3,60\%)_{\text{selling}} \Rightarrow (i',3,60\%,i',4,100\%)_{\text{charging}} \Rightarrow (i',4,100\%,i',5,0\%)_{\text{swapping}}$. Box chains provide a concise reflection of the stocked battery operations. Thus, determining the optimal schedule for stocked batteries equates to finding the most favorable box chains. Considering the pool of feasible box chains available, the formulation presented in Sections 4.2.1 and 3.2 can be stated as the following master problem ([MP]):

$$\max \quad \sum_{a \in A^{\text{rent}} \cup A^{\text{sell}}} p_a x_a - \sum_{a \in A^{\text{relo}} \cup A^{\text{charg}}} c_a x_a + \sum_{i \in I^{[2]}, u \in U} c^{\text{chain}}_{i,u} g_{i,u} \tag{15}$$

s.t. Constraints (2), (4), (5)

$$\sum_{a \in \xi^{+}_{i,t,e} \setminus A^{\text{swap}}} x_a + \sum_{u \in U,\, a \in \zeta^{+}_{i,t,e} \cap A^{\text{swap}}} \delta^{a}_{i,u} g_{i,u} - \sum_{a \in \zeta^{-}_{i,t,e} \setminus A^{\text{swap}}} x_a - \sum_{u \in U,\, a \in \zeta^{-}_{i,t,e} \cap A^{\text{swap}}} \delta^{a}_{i,u} g_{i,u} = 0, \quad \forall i \in I,\, t \in T^{[1]},\, e \in E \tag{16}$$

$$\sum_{a \in A^{\text{start}}_{i,t} \cap A^{\text{park}} \setminus A^{\text{swap}}} x_a + \sum_{u \in U,\, a = (n_{i,t,0}, n_{i,t+1,|E|}) \in A^{\text{swap}}} \delta^{a}_{i,u} g_{i,u} \le m_i, \quad \forall i \in I, t \in T \tag{17}$$

$$\sum_{u \in U, b = (n_{i,0,e}, n_{i,1,e}) \in B^{\text{source}}} \delta^{b}_{i,u} g_{i,u} = \lambda^{B}_{i,0,e}, \ \forall i \in I^{[2]}, e \in E \tag{18}$$

$$x_a, g_{i,u} \in \mathbb{Z}_{\ge 0}, \ \forall a \in A, i \in I^{[2]}, u \in U \tag{19}$$

where U represents the set of feasible chains, and $\delta^{a}_{i,u}(\delta^{b}_{i,u})$ is an indicator parameter signifying the presence of arc $a \in A^{\text{swap}}(b \in B^{\text{source}})$ within chain u at station i. $c^{\text{chain}}_{i,u}$ denotes the profit from chain u of boxes at station i. The parameters are derived from the solution

Table 5
Additional variables and parameters used in the pricing problem for boxes at station $i \in I^{[2]}$.

Sets	Description
H_i^{sell}	Set of energy selling status arcs of a box at station $i \in I^{[2]}$, representing the status whereby a box contains a battery that is selling energy, $H_i^{\text{sell}} = \left\{\left(n_{i,t,e}, n_{i,t+1,r}\right) \middle\| t \in T^{[1]}, e, r \in E, r = \max(0, e - \beta^{\text{D}})\right\}$
H_i^{charg}	Set of charging status arcs of a box at station $i \in I^{[2]}$, representing the status whereby a box contains a battery that is being charged, $H_i^{\text{charg}} = \left\{\left(n_{i,t,e}, n_{i,t+1,r}\right) \middle\| t \in T^{[1]}, e, r \in E, r = \min(e + \beta_{i,t,e}^{\text{C}}, \|E\|)\right\}$
H_i^{idle}	Set of idle status arcs of a box at station $i \in I^{[2]}$, representing the status whereby a box contains a battery that is idle, $H_i^{\text{idle}} = \left\{\left(n_{i,t,e}, n_{i,t+1,e}\right) \middle\| t \in T^{[1]}, e \in E\right\}$
H_i^{swap}	Set of swapping battery status arcs of a box at station $i \in I^{[2]}$, representing the status whereby a box contains a battery that is replacing a depleted vehicle-stalled battery, $H_i^{\text{swap}} = \left\{\left(n_{i,t,\|E\|}, n_{i,t+1,0}\right) \middle\| t \in T^{[1]}\right\}$
H_i^{source}	Set of dummy source arcs of a box at station $i \in I^{[2]}$, $H_i^{\text{source}} = \left\{\left(n_{i,0,e}, n_{i,1,e}\right) \middle\| e \in E\right\}$
H_i	Set of all status arcs of a box at station i, $H_i = H_i^{\text{sell}} \cup H_i^{\text{charg}} \cup H_i^{\text{idle}} \cup H_i^{\text{swap}}$
$\Phi_{i,t,e}^{+}$, $\Phi_{i,t,e}^{-}$	Set of status arcs for which $n_{(i,t,e)}$ is the destination and origin node, respectively
Parameters	**Description**
$\pi_{i,t,e}^{[1]}$, $\pi_{i,t}^{[2]}$, $\pi_{i,e}^{[3]}$	Dual values
p_h	Revenue from status arc $h \in H$, with a definition consistent with p_b in Section 3.2
c_h	Cost of arc $h \in H$, with a definition consistent with c_b in Section 3.2
Decision variables	**Description**
f_h	Binary variables, 1 if status arc $h \in H$ is selected to compose a chain, and 0 otherwise

of the pricing subproblem, which will be presented in the following subsection. $g_{i,u}$ is the decision variable, representing the number of boxes at station i selecting chain u. It should be noted that each used box matches a single chain, but one station could be linked with more than one chain when it accommodates multiple used boxes. Hence, decision variable is a non-negative integer variable. Furthermore, it is worth mentioning that different boxes can potentially share the same chain, implying that the status of these boxes remains equal throughout the operational timeframe.

The objective function continues to have the same meaning as in [P]. The term $\sum_{i \in I^{[2]}, u \in U} c_{i,u}^{\text{chain}} g_{i,u}$ is equal to $\sum_{b \in B^{\text{sell}}} p_b y_b - \sum_{b \in B^{\text{charg}} \cup B^{\text{swap}}} c_b y_b$. Since the composition of each chain is known in advance, the value of $c_{i,u}^{\text{chain}}$ can be precomputed. Constraints (16)–(18) are equivalent to Constraints (3), (6) and (7), respectively, but reformulated in terms of the variable $g_{i,u}$ instead of y_b and x_a ($a \in A^{\text{swap}}$). Constraints (19) impose that decision variables x_a and $g_{i,u}$ are non-negative integer values.

While [MP] is equivalent to [P], as the problem size increases, the number of feasible chains might experience exponential growth, creating a significant challenge for solving. Moreover, it becomes impossible to enumerate all feasible chains. To address this concern, CG solves the restricted master problem ([RMP]), which involves a subset of feasible chains, enabling a more manageable computation. Within the iteration process of CG, new promising columns are generated using information from the dual variables. To achieve this, the relaxation of [RMP] ([RMLP]) is tackled. In this relaxed formulation, Constraints (19) are relaxed to continuous variables ($x_a, g_{iu} \geq 0$). This relaxation enhances the exploration of potential solutions and contributes to the computational efficiency.

4.2.3. Pricing problem

To formulate the pricing problem for boxes at station $i \in I^{[2]}$, an expanded notation is introduced, as shown in Table 5.

After solving [RMLP], the dual values for Constraints (16)–(18) can be obtained. Let $\pi_{i,t,e}^{[1]}$ ($i \in I^{[2]}, t \in T^{[1]}, e \in E$) represent the dual values of Constraints (16), $\pi_{i,t}^{[2]}$($i \in I^{[2]}, t \in T$) represent the dual values of Constraints (17), and $\pi_{i,e}^{[3]}$ ($i \in I^{[2]}, e \in E$) represent the dual values of Constraints (18). For each station $i \in I^{[2]}$, the reduced cost of column u in [RMLP] can be formulated as follows:

$$\begin{aligned}\bar{c}_{i,u} = c_{i,u}^{\text{chain}} &- \sum_{t \in T^{[1]}, e \in E} \pi_{i,t,e}^{[1]} \left(\sum_{a \in \zeta_{i,t,e}^{+} \cap A^{\text{swap}}} \delta_{i,u}^{a} - \sum_{a \in \zeta_{i,t,e}^{-} \cap A^{\text{swap}}} \delta_{i,u}^{a} \right) \\ &+ \sum_{t \in T} \pi_{i,t}^{[2]} \sum_{a = (n_{i,t,0}, n_{i,t,|E|}) \in A^{\text{swap}}} \delta_{i,u}^{a} \\ &+ \sum_{e \in E} \pi_{i,e}^{[3]} \sum_{b = (n_{i,0,e}, n_{i,1,e}) \in B^{\text{source}}} \delta_{i,u}^{b}\end{aligned} \tag{20}$$

where

$$c_{i,u}^{\text{chain}} = \sum_{h \in H_i^{\text{sell}}} p_h f_h - \sum_{h \in H_i^{\text{charg}} \cup H_i^{\text{swap}}} c_h f_h \tag{21}$$

By performing the necessary substitutions and collecting terms, this reduced cost can be expressed as follows:

$$\begin{aligned}\bar{c}_{i,u} = & \sum_{h\in H_i^{\text{sell}}} p_h f_h - \sum_{h\in H_i^{\text{charge}}\cup H_i^{\text{swap}}} c_h f_h \\ & - \sum_{t\in T^{[1]}} \sum_{h=(n_{i,t,|E|},n_{i,t+1,0})\in H_i^{\text{swap}}} \left(\pi_{i,t,|E|}^{[1]} - \pi_{i,t,0}^{[1]}\right) f_h \\ & + \sum_{t\in T} \sum_{h=(n_{i,t,|E|},n_{i,t+1,0})\in H_i^{\text{swap}}} \pi_{i,t}^{[2]} f_h \\ & + \sum_{e\in E} \sum_{h=(n_{i,0,e},n_{i,1,e})\in H_i^{\text{source}}} \pi_{i,e}^{[3]} f_h \end{aligned} \tag{22}$$

In each iteration of the CG process, $\left|I^{[2]}\right|$ pricing subproblems are solved, with each subproblem associated with a specific station $i \in I^{[2]}$. A feasible solution to a pricing subproblem corresponds not only to a feasible chain for a box, but also to an element in the set U of [MP]. The pricing problem is to find a promising column with a positive reduced cost, which subsequently is added to [RMLP]. The formulation of the subproblem for each station can be presented as an integer linear program, as detailed below.

[SP$_i$]:

$$\begin{aligned}\max \quad & \sum_{h\in H_i^{\text{sell}}} p_h f_h - \sum_{h\in H_i^{\text{charge}}\cup H_i^{\text{swap}}} c_h f_h - \sum_{t\in T^{[1]}} \sum_{h=(n_{i,t,|E|},n_{i,t+1,0})\in H_i^{\text{swap}}} \left(\pi_{i,t,|E|}^{[1]} - \pi_{i,t,0}^{[1]}\right) f_h \\ & + \sum_{t\in T} \sum_{h=(n_{i,t,|E|},n_{i,t+1,0})\in H_i^{\text{swap}}} \pi_{i,t}^{[2]} f_h + \sum_{e\in E} \sum_{h=(n_{i,0,e},n_{i,1,e})\in H_i^{\text{source}}} \pi_{i,e}^{[3]} f_h \end{aligned} \tag{23}$$

$$\text{s.t.} \quad \sum_{h\in H_i^{\text{source}}} f_h = 1 \tag{24}$$

$$\sum_{h\in \Phi_{i,t,e}^{+}} f_h = \sum_{h\in \Phi_{i,t,e}^{-}} f_h, \quad \forall t \in T^{[1]},\, e \in E \tag{25}$$

$$f_h \in \{0,1\}, \quad \forall h \in H \tag{26}$$

Constraint (24) restricts the battery in a box to have a specific initial SOC during the initial time interval. This ensures that the battery inside the box starts with a defined charge level. Constraints (25) ensure the conservation of status of a box at node $n_{i,t,e}$. Constraints (24) and (25) together ensure that a box only has one status arc within any time interval. Constraints (26) impose binary conditions on the variable f_h. The non-zero solutions of f_h, arranged in ascending order of time, form a chain of boxes at station i.

Since each subproblem is solved separately for each station, the complexity of the problem is significantly reduced. The termination criterion for the CG iteration is met when the largest computed reduced cost, denoted as $\bar{c}^* = \max_i \bar{c}_{i,u}$, is negative. In general, after terminating the CG algorithm, if the current solution to [RMLP] is non-integer, the branch and bound method should be incorporated into the CG technique, known as the branch and price algorithm. Our experimentation with this algorithm has faced challenges, primarily in the selection of effective branching rules due to the high dimensionality of the decision variables. The absence of effective branching rules leads to a large execution time. Consequently, we directly solve the [RMP] with the current column set (Du et al., 2014). After solving the [RMP], we obtain the final near-optimal solution of the original problem. The proposed algorithm can sometimes find the optimal solution. When solving the [RMP], if the chains selected in the optimal solution of the original problem are also part of the current chain set, the proposed algorithm can discover optimal solutions to the original problem. The framework of the proposed CG-based heuristic algorithm is shown in Fig. 4.

4.2.4. *Accelerating techniques*

Column elimination. When the number of columns in [RMLP] becomes too large, a subset of the non-basic columns can be removed. Specifically, columns that have not entered the basis of the master problem in the last η iterations (where η is a predefined parameter) are considered for removal. To ensure proper convergence of the CG process, this elimination procedure should not be performed frequently, and a certain number of non-basic columns should remain in [RMLP] after column removal.

Diversity. Column diversity aids in comprehensively exploring the solution space, thereby increasing the chances of finding the optimal solution. In this study, we use the number of swaps in a chain to describe the diversity. When solving the pricing subproblem, Constraint (27) is added.

$$\sum_{h\in H_i^{\text{swap}}} f_h \geq \kappa \tag{27}$$

Constraint (27) guarantees that at least κ battery swaps happen within a box, where κ is a parameter. The value of this parameter ranges from 1 to $\lfloor |T|/\alpha \rfloor + 1$, where α is the time required for a battery to be continuously charged from empty to full, and $\lfloor |T|/\alpha \rfloor + 1$ represents the maximum number of battery swaps that occur at a box. We assign various values to the parameter κ, with each value corresponding to a distinct subproblem model. These models can be solved in parallel.

Multiple columns. To reduce the number of iterations, at each iteration, we add more than one column with a positive reduced cost (if any). It is not necessary to find the chain with the maximal reduced cost, as long as the reduced cost of the chain is greater

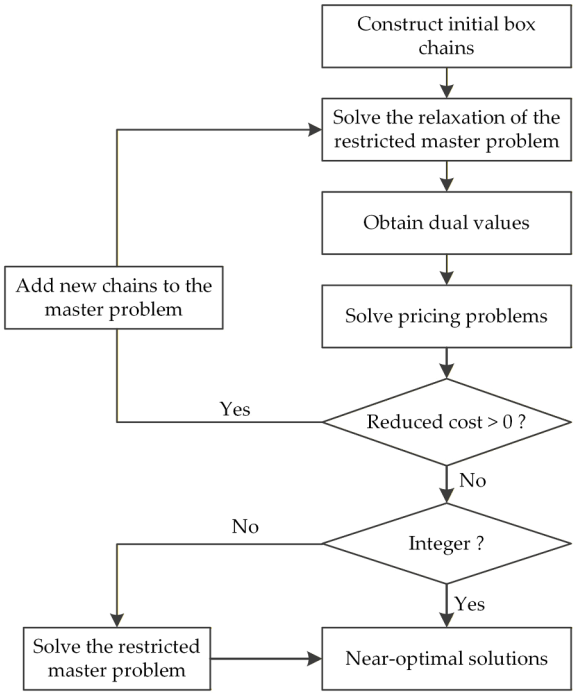


Fig. 4. Framework of the CG-based heuristic algorithm.

than 0, the objective function of [RMLP] can be improved. It should be noted that in our study, each pricing subproblem [SP_i] is solved directly using the commercial integer programming solver CPLEX. This choice is justified by the fact that the model maintains a manageable number of variables and constraints even at larger scales, and our preliminary computational experiments demonstrate that CPLEX can effectively solve the subproblems considered in this study. Notably, this solution strategy aligns with approaches adopted in previous studies, such as Xiao et al. (2022) and Du et al. (2014).

In the computational experiments, we use the solution pool feature provided by CPLEX solver to collect multiple solutions, whether they are optimal or not, generated throughout the optimization process when solving [SP_i]. However, it should also be noted that, if too many columns are added to each iteration, the size of [RMLP] will become increasingly larger, subsequently extending the solution time accordingly.

Relaxation. Based on our preliminary experiments, we observe that the [RMLP] yields integral optimal solutions for a subset of instances. This phenomenon is mainly attributed to the network-flow-like structure embedded in the model. Moreover, we identify a special structural property of [RMP]: when a subset of decision variables is fixed to integer values, the resulting constraint matrix becomes totally unimodular, which guarantees the integrality of the remaining variables. This property is stated as a proposition and proved in Appendix A. Therefore, in the final iteration for obtaining a near-optimal solution to the original problem, we first solve the [RMLP]. If the resulting solution is integral, it is accepted as the final solution; otherwise, we solve the corresponding integer [RMP] in the last iteration.

4.3. Rolling horizon framework

Since request announcements can arrive at any time during the day, the decision-maker cannot access the full-day information in advance. This creates a dynamic optimization problem, where decisions must be made in real-time under partial and evolving information. To address this problem, we adopt the rolling horizon approach, which has been widely applied in real-time and on-demand systems (Agatz et al., 2011; Cordeau et al., 2015; Marufuzzaman et al., 2016; Shui and Szeto, 2018; Liang et al., 2020).

Fig. 5 shows the rolling horizon framework adopted in this paper. This approach operates by dividing the operational timeframe into smaller time windows and solving the optimization problem progressively as time moves forward. The framework enables sequential optimization, where input demand data is processed in batches at regular intervals. The optimization mechanism is executed periodically using the data currently available, without requiring prior knowledge of future demand. As shown in Fig. 5, at each stage w, the current time t_w, rolling period T_w^{roll} and look-ahead period T_w^{ahead}, are three key parameters. The total optimization period at stage w comprises both T_w^{roll} and T_w^{ahead}. Before the current time t_w, precisely within the rolling period of stage $w-1$, users make reservations for departures no earlier than t_w and no later than t_{w+1}. Hence, the rolling period of stage $w-1$ is also the reservation period of stage w. Requests are then evaluated to determine if they will be served at stage w. Once the optimization model is solved for stage w, only activities scheduled to depart within the rolling period T_w^{roll} are implemented, whereas those falling within the look-

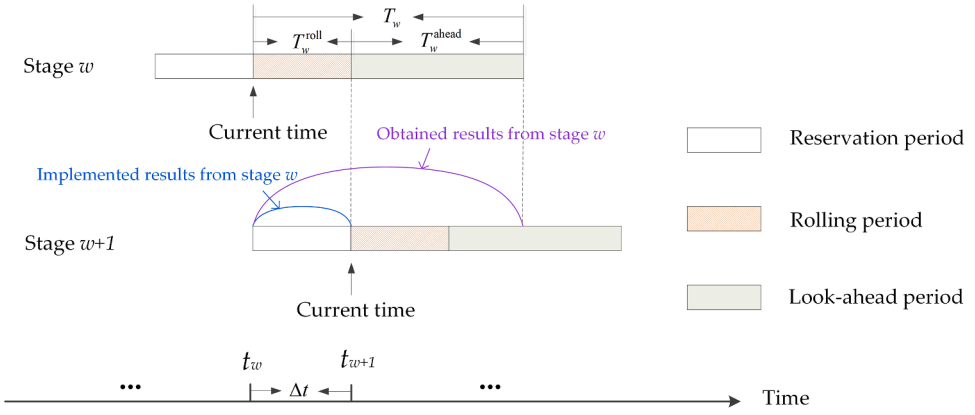


Fig. 5. Illustration of the rolling horizon strategy.

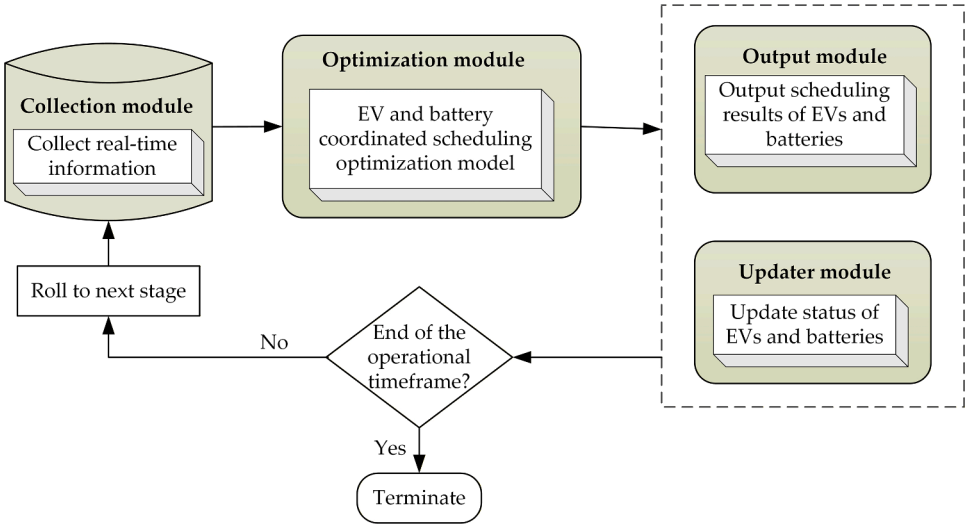


Fig. 6. The rolling horizon-based solution framework.

ahead period are not executed. The framework then advances by Δt time intervals to the next stage, repeating this process iteratively until the end of the operational timeframe is reached.

As shown in Fig. 6, the solution framework consists of four sub-modules: data collection module, optimization module, updater module and output module.

Data collection module: Before each run, the data collection module gathers real-time request data and transmits it to the optimization module. Additionally, this module can collect real-time road travel time and grid fluctuations, enabling the system to account for current traffic conditions and variations in charging power.

Optimization module: The optimization module is a key component of this algorithm, which optimizes the scheduling of SEVs and batteries. The model proposed in Section 3 covers the entire operational timeframe. If it is split into several sub-problems according to the time dimension without making other model adjustments, the effect of the look-ahead period on the next stage would not be considered, so some changes should be imposed on constraints to ensure the continuity between stages. Specifically, set T and $T^{[1]}$ are replaced by T_w ($T_w = \left\{t_w, \ldots, t_w + \left|T_w^{\text{roll}}\right| + \left|T_w^{\text{ahead}}\right|\right\}$) and $T_w^{[1]}$ ($T_w^{[1]} = \left\{t_w, \ldots, t_w + \left|T_w^{\text{roll}}\right| + \left|T_w^{\text{ahead}}\right| - 1\right\}$), respectively. For simplicity, let τ_w^{end} denote the end time interval of stage w ($t_w + \left|T_w^{\text{roll}}\right| + \left|T_w^{\text{ahead}}\right|$). Due to some EVs not being able to reach their destinations within the rolling period of the stage $w-1$, the flow conservation Constraints (3) and (16) are replaced by Constraints (28) and (29) at stage w, respectively. In these constraints, $s_{i,t,e}$ represents the number of vehicles whose departure time was determined in the previous stage $w-1$ to fall within the rolling period but whose arrival time falls within the look-ahead period, as calculated in Eq. (30).

$$\sum_{a \in \zeta_{i,t,e}^{+}} x_a + s_{i,t,e} - \sum_{a \in \zeta_{i,t,e}^{-}} x_a = 0, \quad \forall i \in I,\ t \in T_w^{[1]},\ e \in E \tag{28}$$

$$\sum_{a\in\zeta^{+}_{i,t,e}\setminus A^{\text{swap}}} x_a + \sum_{u\in U,\, a\in\zeta^{+}_{i,t,e}\cap A^{\text{swap}}} \delta^{a}_{i,u} g_{i,u} + s_{i,t,e} - \sum_{a\in\zeta^{-}_{i,t,e}\setminus A^{\text{swap}}} x_a - \sum_{u\in U,\, a\in\zeta^{-}_{i,t,e}\cap A^{\text{swap}}} \delta^{a}_{i,u} g_{i,u} = 0, \quad \forall i \in I,\, t \in T^{[1]}_{w},\, e \in E \tag{29}$$

$$s_{i,t,e} = \begin{cases} \sum_{a\in\left\{(n_{j,k,r},n_{i,t,e})\in A^{\text{rent}}\cup A^{\text{relo}} \mid k\in T^{\text{roll}}_{w-1}\right\}} x_a, & \text{if } t \in T^{\text{ahead}}_{w-1} \\ 0, & \text{else} \end{cases} \tag{30}$$

Updater module: After solving the optimization model for stage w, the variables related to activities with start times within the rolling period are treated as fixed parameters for the next run. These fixed values are then used to update the initial locations and statuses of EVs, as well as the battery statuses for the next stage $w+1$. The updates follow Eqs. (31) and (32).

$$\lambda^{V}_{i,t_{w+1}-1,e} = \sum_{a\in\zeta^{+}_{i,\tau^{\text{end}}_{w},e}} x_a + s_{i,\tau^{\text{end}}_{w},e}, \quad \forall i \in I,\, e \in E \tag{31}$$

$$\lambda^{B}_{i,t_{w+1}-1,e} = \sum_{a\in\theta^{+}_{i,\tau^{\text{end}}_{w},e}} y_a, \quad \forall i \in I^{[2]},\, e \in E \tag{32}$$

Output module: This module ensures the timely execution of optimized scheduling decisions for SEVs and stocked batteries resources. Only those decisions that are scheduled to take place within the current rolling period are implemented.

As mentioned earlier, our demand input strategy adopts a batch processing approach, which is a common practice in rolling horizon methods (Levin et al., 2019; Liang et al., 2020; Zhen et al., 2023). While our framework employs this strategy, it also supports an alternative strategy of integrated prediction. Specifically, demand forecasting can be incorporated into the data collection module, enabling it to combine both actual reservations with departure times falling within the rolling period and predicted demand within the look-ahead period at each stage. This aggregated data is then fed into the optimization module. The remaining modules in the framework do not require modification under this alternative strategy.

5. Numerical experiments

In Section 5.1, we test a set of numerical instances to validate the proposed algorithm. Furthermore, in Section 5.2, we perform a series of sensitivity analyses based on a real-world case in the city of Lanzhou, Gansu, China, to identify key parameters and assess their impact on the system's performance. All experiments are carried out using a personal laptop equipped with an Intel Core i5 processor running at 2.4GHz and 16 GB of RAM.

5.1. Computational performance of the solution method

In this section, we assess the performance of the proposed CG-based heuristic algorithm through 20 randomly generated instances. The effectiveness of the algorithm is evaluated in comparison to solutions obtained solely using the CPLEX solver. Our computations are executed under a predefined maximum computation time of 3600 seconds. If no feasible solution is found within 3600 seconds, the objective value and optimality gap reported by CPLEX are denoted as "NA". The summarized results are presented in Table 6.

In Table 6, Column 1 denotes the instance index, and Column 2 describes the problem scale represented by a triple (number of stations, number of time intervals, number of demand). Columns 3-5 present the objective value, computational time, and optimality gap obtained by CPLEX, respectively. Columns 6 and 7 report the objective value and computational time of the CG-based heuristic algorithm, and Column 8 reports the objective value gap between the two approaches, defined as follows:

$$\text{Obj. gap} = \frac{\gamma^{CPLEX} - \gamma^{CG}}{\gamma^{CPLEX}} \times 100\% \tag{33}$$

where γ^{CPLEX} represents the objective value of [P] by CPLEX, γ^{CG} represents the objective value of [P] by proposed CG-based heuristic algorithm.

Analyzing the data in Table 6, we observe that both solution approaches require increased computational time as the instance scale grows. Notably, the performance of CPLEX solutions deteriorates more rapidly compared to that of the CG-based heuristic algorithm. For small- and medium-sized instances (Instances 1-6), CPLEX is able to solve problems to optimality within relatively short computational times, with zero optimality gaps. In these cases, the CG-based heuristic algorithm also achieves optimal or near-optimal solutions, with an average objective value gap of 0.81%, although its computational time is generally longer than that of CPLEX for small instances.

As the problem scale increases (Instances 7-14), CPLEX remains capable of finding high-quality solutions, but its computational time grows rapidly, exceeding 2000 seconds for several instances. In contrast, the CG-based heuristic algorithm consistently requires substantially less computational time, achieving an average reduction of approximately 59% in solution time. Although objective gaps increase as the problem scale grows, they remain within a reasonable range (mostly below 10%, averaging 6.99%), demonstrating a favorable trade-off between solution quality and computational efficiency.

Table 6
Computational performance of the two solution approaches.

Instances	Problem scale	CPLEX			CG-based heuristic algorithm		
		Obj.	Time (s)	Gap (%)	Obj.	Time (s)	Obj. Gap (%)
1	10-10-100	1982.00	2.36	0.00	1982.00	9.57	0.00
2	20-10-400	5157.00	19.74	0.00	5157.00	50.81	0.00
3	10-20-300	4717.00	21.23	0.00	4717.00	47.15	0.00
4	15-20-300	6416.00	114.58	0.00	6383.00	84.41	0.51
5	30-10-300	6656.50	125.76	0.00	6540.00	89.58	1.75
6	20-20-500	8983.50	274.03	0.00	8749.00	122.62	2.61
7	30-15-400	9476.00	286.36	<0.10	9076.00	121.19	4.22
8	20-30-500	12,203.00	1063.87	<0.10	11,790.00	279.06	3.38
9	50-10-500	11,191.50	656.62	<0.10	10,670.50	245.93	4.66
10	70-10-1000	17,217.00	1189.69	<0.10	16,024.50	440.12	6.93
11	40-20-1000	18,268.50	1657.82	<0.10	16,797.00	519.32	8.05
12	60-15-1000	20,217.50	2085.41	<0.10	18,324.00	790.29	9.37
13	70-15-1200	23,820.50	2770.86	<0.10	21,746.50	926.18	8.71
14	30-30-1000	21,565.00	3349.56	<0.10	19,273.00	1079.33	10.63
15	60-20-1500	27,492.00	>3600.00	5.94	27,285.00	1318.23	0.75
16	50-20-800	21,246.50	>3600.00	4.46	21,171.50	1789.91	0.42
17	70-20-1500	30,007.00	>3600.00	9.67	30,261.50	2334.35	-0.85
18	60-30-2000	NA	>3600.00	NA	40,300.50	2694.89	NA
19	70-30-2000	NA	>3600.00	NA	44,014.00	2763.52	NA
20	60-40-2500	NA	>3600.00	NA	47,111.00	2807.43	NA

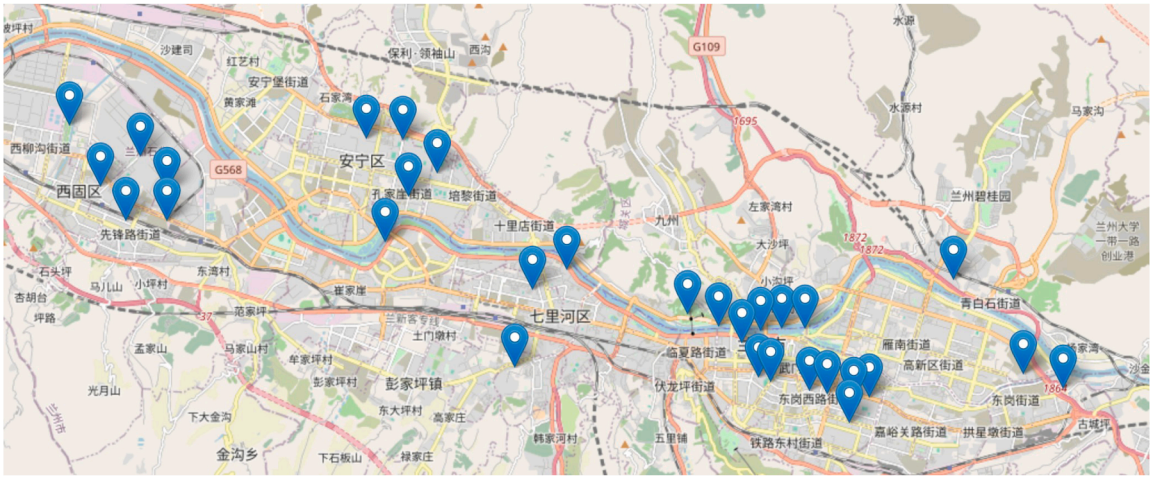


Fig. 7. Exiangxing station locations in the city of Lanzhou.

For large-scale instances (Instances 15-20), CPLEX is unable to reach optimality within the 3600-second time limit and, in some cases, fails to identify a feasible solution. In these challenging cases, the proposed algorithm continues to yield satisfactory solutions within acceptable computational times. Notably, for Instance 17, the heuristic outperforms the solution obtained by CPLEX within 2500 seconds, resulting in a negative objective value gap.

Overall, these results indicate that the proposed algorithm is able to find high-quality solutions within reasonable computational times and that its performance notably surpasses that of the commercial solver for larger instances. Since the demand of instances in Table 6 is input to the model collectively and solved in a single run without using the rolling horizon method, any of these instances can be viewed as the optimization model solved at a certain stage of the rolling horizon algorithm or regarded as a special case where the length of the optimization period equals the entire operational timeframe.

5.2. Case study and sensitivity analysis

Exiangxing is a station-based carsharing company founded in 2017 in Lanzhou, China, offering both one-way and round-trip services. In the following case studies, real-world operational data from Exiangxing are used to evaluate the effectiveness of the proposed method. The original dataset covers August 2018. For analysis, we select the 30 stations with the highest demand during this month and their spatial distribution is shown in Fig. 7.

Fig. 8a illustrates the cumulative demand at the selected 30 stations over August, while Fig. 8b presents the demand profile of a representative day. Fig. 8c further shows the hourly OD demand among these 30 stations during a day. Notably, the demand

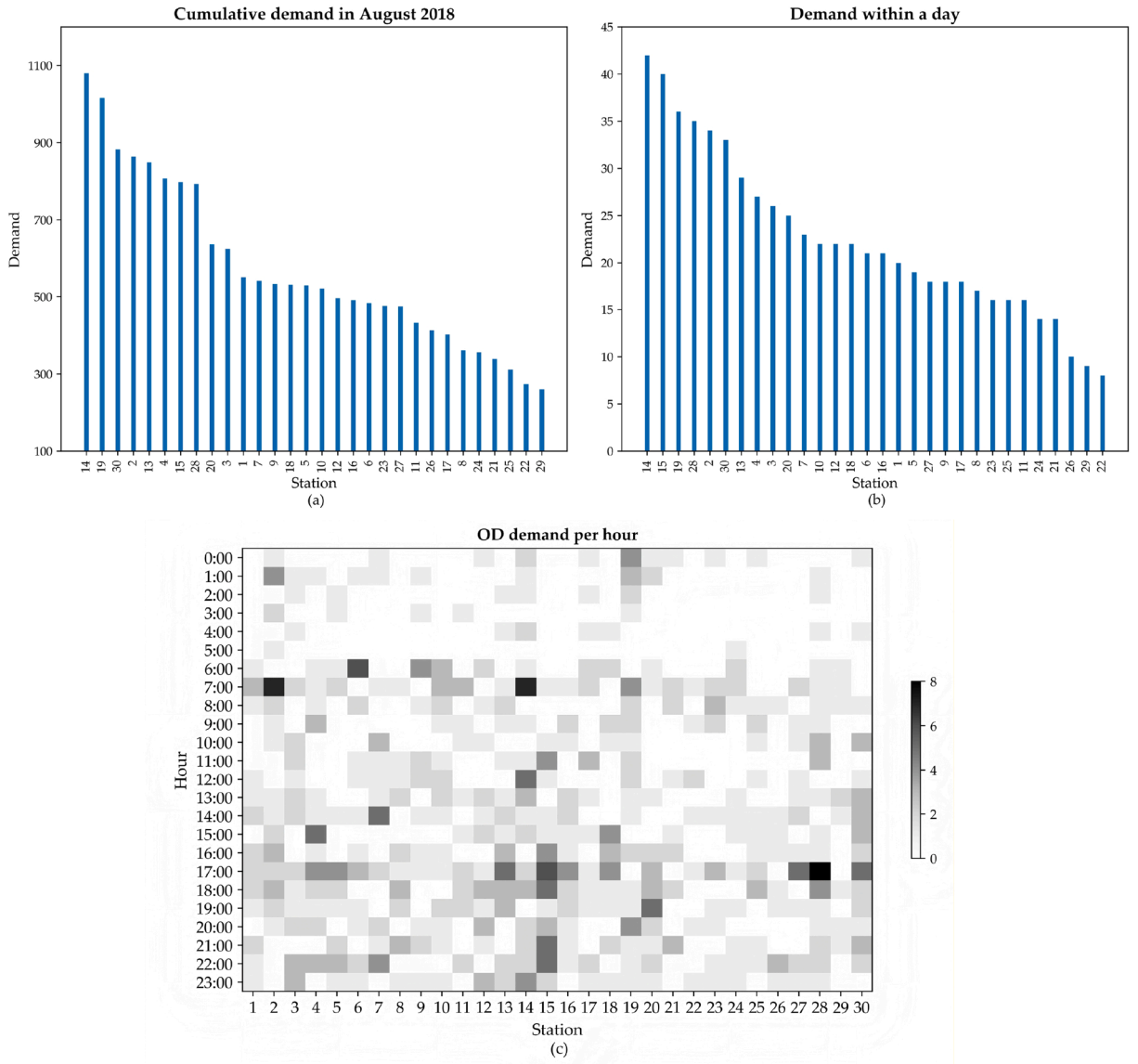


Fig. 8. Monthly, daily and hourly demand.

distribution is imbalanced, with peak periods occurring in the morning and evening. Accordingly, the study period of the case study is set from 7:00 a.m. to 7:00 p.m., covering both peak and off-peak hours. SOC levels are discretized into the following levels: {0%, 10%, 20%, 30%, 40%, 50%, 60%, 70%, 80%, 90%, 100%}. The parameters used in the case study are based on the Exiangxing operational data, and their values are summarized in Table 7. To generate demand data, we employ a roulette-wheel selection method based on historical statistical distribution. In the following parameter analysis, each performance indicator is derived from 20 independent computations, where demand is regenerated in each run, and the initial distribution of vehicles and batteries is randomized. The results are reported either as average values or illustrated using box plots in this section.

5.2.1. Sensitivity analysis on the rolling horizon parameters

In this section, we conduct a series of sensitivity analyses with different parameter values for the rolling horizon approach to evaluate their impact on system performance. Specifically, we examine multiple combinations of rolling periods (10-60 minutes) and look-ahead periods (30-70 minutes). In this analysis, the length of each time interval is set to 10 minutes.

Fig. 9 illustrates the profit outcomes, showing that longer rolling and look-ahead periods improve profitability. This suggests that a longer optimization period at each stage leads to more effective vehicle allocations and higher revenue. Notably, a threshold effect is observed: beyond a rolling period of 40 minutes and a look-ahead period of 50 minutes, profit growth slows. For instance, increasing

Table 7
Parameter settings in the case study.

Number of time intervals	52
Number of stations	30
Length of a time interval	15 min
Fleet size	90
Quantity of total demand	1000
Operational timeframe	7:00 - 19:00
Electricity price in peak periods	0.759 CNY/kWh
Electricity price in off-peak periods	0.261 CNY/kWh
Electricity price in flat-peak periods	0.51 CNY/kWh
Rental fee	0.8 CNY/min
Relocation cost	0.4 CNY/min
Swapping cost	5 CNY
Battery capacity	20 kWh
Number of parking spaces in a station	5

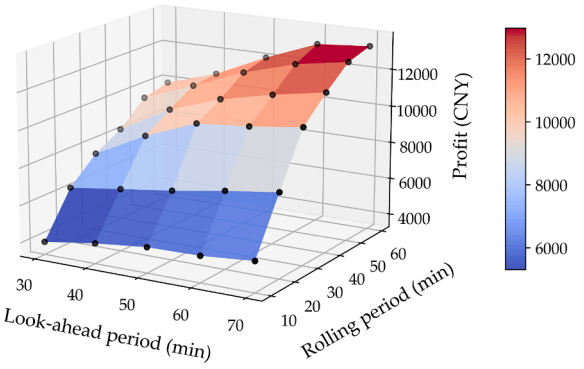


Fig. 9. Performance comparison across different combinations of rolling and look-ahead periods.

the rolling horizon from 10 to 20 minutes results in an average profit increase of 55.37%, whereas extending it from 40 to 50 minutes yields a much smaller increase of only 3.06%.

In this study, the length of the rolling period is set equal to that of the reservation period, representing the degree of advance booking flexibility provided to users. From a managerial perspective, extending the reservation period enables operators to better anticipate demand, process requests more efficiently, and optimize vehicle allocation, thereby improving overall profitability. However, excessively long reservation horizons may reduce user convenience and limit service accessibility. These findings suggest that operators should carefully calibrate the reservation period to strike a balance between operational efficiency and user experience in reservation-based carsharing systems.

5.2.2. Sensitivity analysis on the charging rate

The charging rate of charging facilities directly impacts vehicle operational efficiency, potentially leading to variations in system performance. In this section, we analyze its effect by conducting a sensitivity analysis across three scenarios: (i) fast charging, (ii) normal charging, and (iii) slow charging. To facilitate this comparison, we adopt the nonlinear charging curve provided by Montoya et al. (2017), which is derived from real charging data provided by Uhrig et al. (2015) and approximated using piecewise linear functions. These charging profiles are depicted in Fig. 10. The results are summarized in Table 8 and Fig. 11, with all values reported as averages.

Table 8 indicates a positive correlation between charging rate and system performance metrics. As charging rate increases, both profit and service rate improve substantially, with profit rising by 13.97% and the service rate by 7.51% from the slowest to the fastest charging scenario. This improvement is primarily driven by the reduction in charging time, which increases vehicle availability for rental services. As expected, the fast-charging scenario exhibits the highest proportion of rental time, reaching 66.37%. While the results presented here focus solely on operational performance and do not explicitly include charging infrastructure costs, fast charging can still be considered economically attractive, provided that the additional daily depreciation of fast-charging facilities relative to other types of infrastructure remains smaller than the corresponding increase in profit generated by fast charging. Specifically, in our case, fast charging yields a profit gain of 532.4 CNY over normal charging and 1624.4 CNY over slow charging, implying that the investment in fast-charging facilities can be justified as long as the higher daily depreciation costs are smaller than these profit gains.

An interesting observation is that the charging rate also significantly impacts battery swapping operations. Under slow-charging conditions, the system exhibits 38.04% longer charging duration for stocked batteries and requires 359.75% more swapping operations compared to fast-charging. This compensatory mechanism occurs because prolonged charging times create bottlenecks in vehicle availability, forcing greater reliance on battery swapping to maintain operational continuity. These findings demonstrate that the

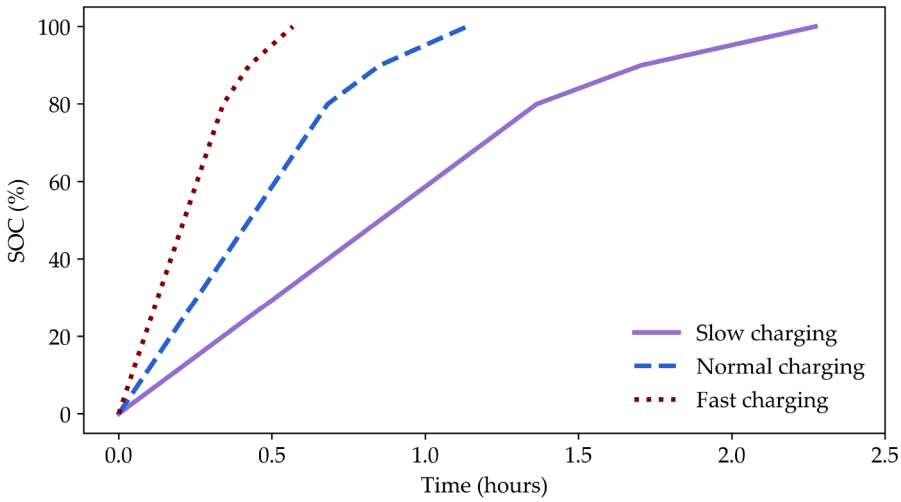


Fig. 10. Charging curves with different charging rates.

Table 8
Sensitivity analysis results using different charging rates.

Indicators	Fast charging	Normal charging	Slow charging
Profit (CNY)	13250.2	12717.8	11625.8
Service rate (%)	75.27	71.01	67.76
Operations of battery swapping	15.9	58.8	73.1
Vehicle time:			
Rental time (%)	66.37	64.94	60.74
Relocation time (%)	5.11	4.31	3.10
Charging time (%)	11.48	13.74	17.11
Energy selling time (%)	2.14	1.11	0.38
Battery swapping time (%)	0.47	1.72	2.14
Idle time (%)	14.43	14.18	16.53
Stocked battery time:			
Charging time (%)	7.98	26.51	46.02
Energy selling time (%)	47.73	44.30	29.58
Battery swapping time (%)	0.93	3.44	4.27
Idle time (%)	43.36	25.75	20.13

charging rate directly affects the system's dependence on battery swapping. Operators should therefore tailor battery management strategies to different charging-rate infrastructure in order to balance operational efficiency and infrastructure utilization.

Fig. 11 illustrates the quantities of charging and selling energy for vehicles and stocked batteries across different hours. The grey bars in the figure represent electricity prices, which fluctuate throughout the study period. Fig. 11a and b present the total charging and energy selling quantities in the system. Fig. 11c and d show the quantities of charging and energy selling for vehicles, and Fig. 11e and f depict the corresponding quantities for stocked batteries. The values shown in Fig. 11c and e for each hour sum up to the values in Fig. 11a, while the values in Fig. 11d and f correspondingly sum up to the values in Fig. 11b. It is evident that during peak electricity price periods, both vehicles and stocked batteries tend to avoid purchasing energy and instead lean towards selling energy. This indicates that V2G and B2G technologies indeed play a role in energy storage and load balancing. Their price-responsive charging and discharging behavior implies that operators can improve economic outcomes and grid stability by actively incorporating electricity price signals into the scheduling of both mobile and stationary batteries.

Since slow charging requires longer charging durations, vehicles cannot replenish energy quickly enough during operation and therefore leads to greater dependence on stocked batteries. This means that more charging operations are needed for the stocked batteries to maintain an adequate supply of spares, resulting in the highest charging demand for stocked batteries under the slow charging mode. In contrast, under the fast-charging strategy, vehicles can fully charge in a short time, making them more likely to charge directly on the vehicle rather than relying on stocked batteries. As seen in Fig. 11c, vehicle charging demand is significantly high under fast charging. This reduces the charging demand for stocked batteries, implying that under fast charging, battery charging mainly serves B2G operations. Combined with the reduced number of battery swaps, the amount of electricity sold is the highest under the fast-charging strategy.

Another noteworthy observation is that SEVs exhibit limited participation in electricity selling. The amount of electricity sold by electric vehicles is less than 15% of that sold by stocked batteries. The revenue generated by SEVs primarily depends on serving

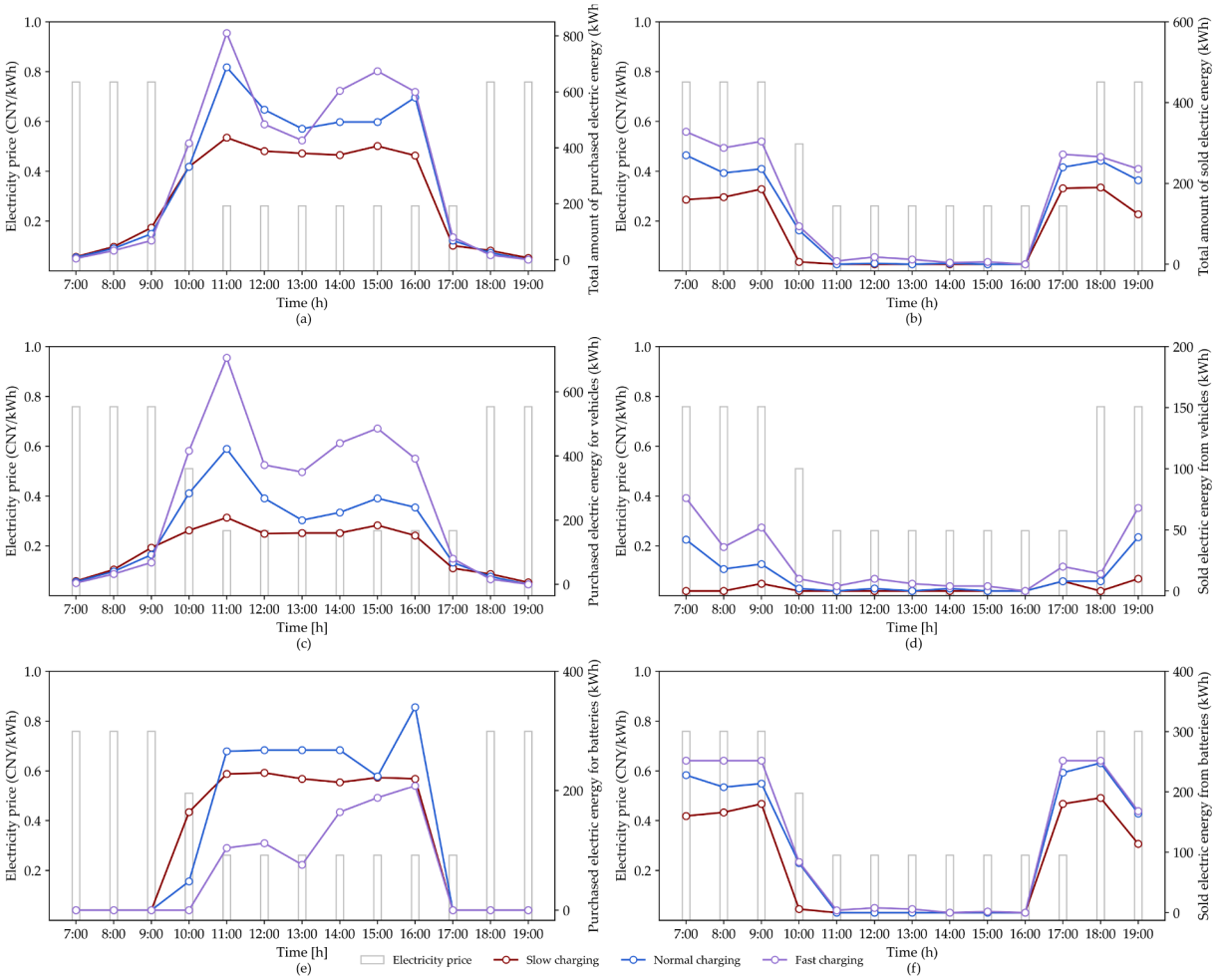


Fig. 11. Charging and energy selling quantity each hour.

carsharing demands. Despite the high electricity prices at 7 a.m. and 6 p.m., which are also peak hours for carsharing, SEVs prioritize serving users. Therefore, the amount of electricity sold by the vehicles during these peak hours is not high. This indicates that the emergence of V2G and B2G does not affect the core business of catering to the travel demands of carsharing services.

5.2.3. *Sensitivity analysis on the fleet size*

In this section, we conduct a sensitivity analysis to examine the effect of fleet size on system performance. In our experimental setup, we consider a range of fleet sizes from 30 to 130 vehicles, with increments of 20. The resulting indicators are presented in Fig. 12. As the fleet size increases, vehicle depreciation costs increase accordingly. This leads to a modification of the profit calculation, which is expressed as follows:

$$\sum_{a\in A^{\text{rent}}\cup A^{\text{sell}}} p_a x_a + \sum_{b\in B^{\text{sell}}} p_b y_b - \sum_{a\in A^{\text{relo}}\cup A^{\text{charg}}} c_a x_a - \sum_{b\in B^{\text{charg}}\cup B^{\text{swap}}} c_b y_b - c^{\text{vehicle}} F \tag{34}$$

where c^{vehicle} is the depreciation cost of a vehicle per day, set at 25 CNY per day and F represents the fleet size.

Fig. 12 illustrates the variation in daily profit, average profit per vehicle, and the number of battery swapping operations as fleet size increases. Total profit increases with fleet size, but the growth rate declines. When the fleet size exceeds 90 vehicles, the profit growth rate decelerates noticeably, demonstrating a saturation effect in fleet expansion. The average profit per vehicle decreases with increasing fleet size due to the underutilization of additional vehicles, resulting in lower revenue per vehicle.

Fig. 12c shows the changes in the number of battery swaps. The battery swapping operation frequency initially rises with increasing fleet size. Within the range of 30 to 70 vehicles, the increase in the number of battery swaps aligns with fleet growth. This is because, at relatively small fleet sizes, the available vehicles are still insufficient to satisfy carsharing demand under operational constraints, making battery swapping an important supplementary mechanism to sustain system operations. However, when the fleet size exceeds 70 vehicles, the system's reliance on battery swapping gradually declines. This finding further confirms that battery swapping serves

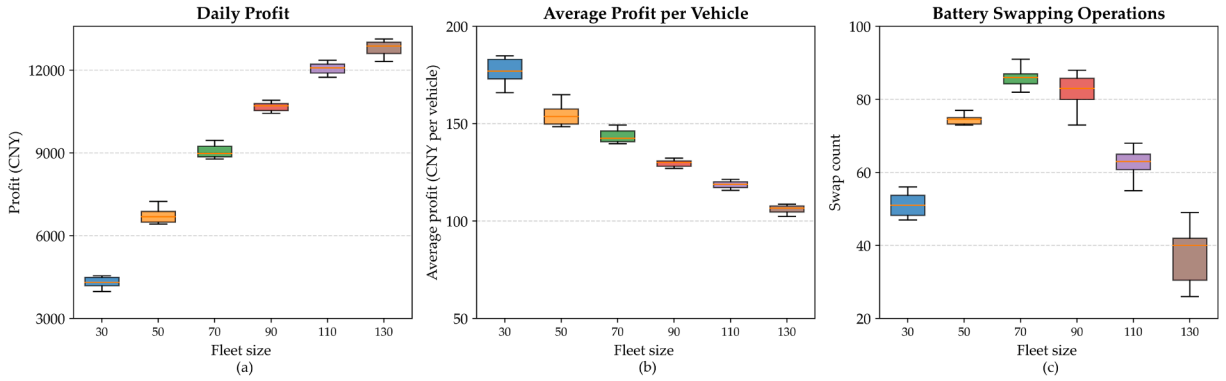


Fig. 12. Results of sensitivity analysis of fleet size.

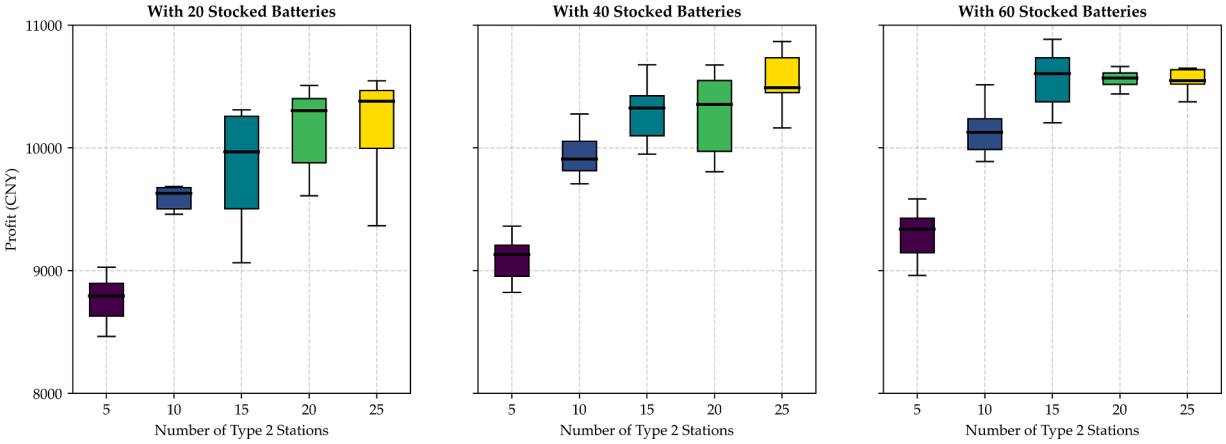


Fig. 13. Results of sensitivity analysis of different number of stocked batteries and Type 2 stations.

as an auxiliary charging method, primarily beneficial in scenarios with limited vehicle availability. As the fleet size increases, the dependency on battery swapping diminishes, and with a sufficiently large fleet, it becomes less critical. These observations indicate that battery swapping facilities are most valuable under limited fleet availability. Operators can therefore prioritize battery swapping deployment in areas with high demand and constrained fleet coverage. In addition, battery swapping can function as a short-term capacity buffer under demand surges or fleet shortages. Incorporating swapping facilities into contingency planning can enhance system resilience without requiring permanent fleet expansion.

5.2.4. Sensitivity analysis on the number of stocked batteries and Type 2 stations

Efficient allocation of stocked batteries and Type 2 stations is crucial for effective resource utilization and affects overall system performance. To explore this relationship, we analyze the impact of different numbers of stocked batteries and Type 2 stations on profitability. In this experiment, we consider three battery stock levels: low (20 stocked batteries), moderate (40 stocked batteries), and high (60 stocked batteries). For Type 2 stations, we evaluate five configurations: 5, 10, 15, 20, and 25 stations. In each computation, Type 2 stations are randomly selected from all 30 stations, and stocked batteries are randomly distributed among them, with the number of batteries per station constrained to a minimum of 1 and a maximum of 15. Due to variations in station and battery numbers, fixed costs differ, and the profit in this analysis is defined as follows:

$$\sum_{a\in A^{\text{rent}}\cup A^{\text{sell}}} p_a x_a + \sum_{b\in B^{\text{sell}}} p_b y_b - \sum_{a\in A^{\text{relo}}\cup A^{\text{charg}}} c_a x_a - \sum_{b\in B^{\text{charg}}\cup B^{\text{swap}}} c_b y_b - c^{\text{battery}} Y - c^{\text{station}} S \tag{35}$$

where c^{battery} represents the daily depreciation cost per battery, fixed at 10 CNY per day, c^{station} is the daily amortized construction cost of a Type 2 station per day, set to 15 CNY per day, Y denotes the number of stocked batteries, and S represents the number of Type 2 stations. The results are shown in Fig. 13.

When the number of stations is limited, overall profit remains low, even with sufficient stocked batteries. For example, distributing 40 batteries across 5 stations yields lower profit than distributing 20 batteries across 10 stations. Similarly, when the number of stocked batteries is fixed, increasing the number of Type 2 stations from 5 to 10 significantly boosts profit. However, beyond 15 stations, further increases yield only marginal profit improvements. Notably, an excessive number of stocked batteries does not always lead to higher profit when more Type 2 stations are available. For instance, with 60 stocked batteries, opening 20 or 25 stations results in

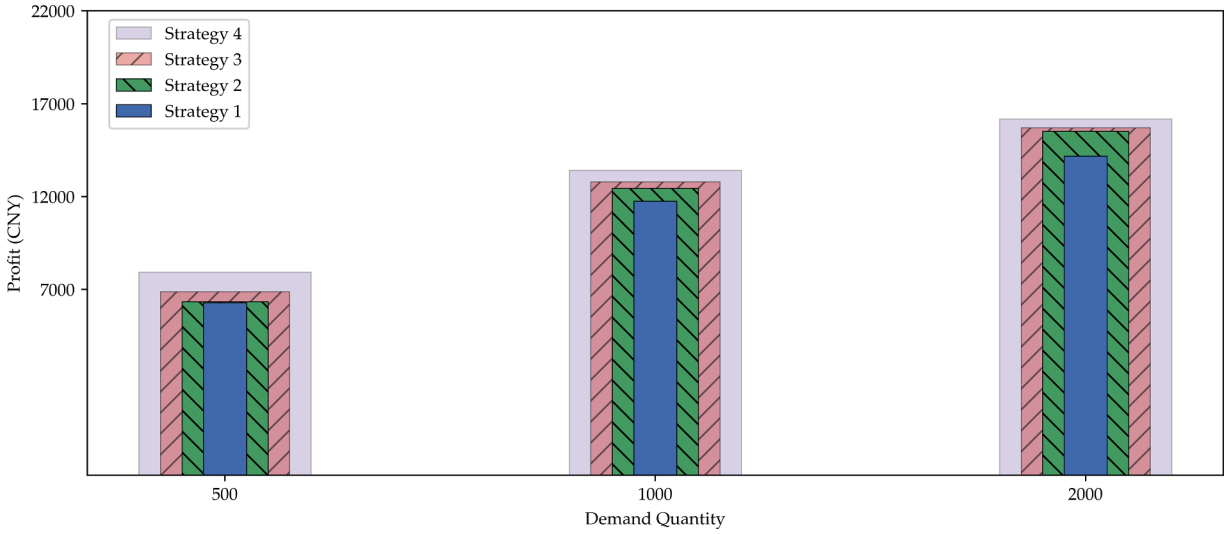


Fig. 14. Results of sensitivity analysis of different energy management strategies.

lower profit than with 15 stations. This suggests that an excessive number of Type 2 stations leads to underutilization and increased fixed costs, highlighting the need for an optimal balance between stocked batteries and station availability. Based on the results, the optimal number of Type 2 stations appears to be around 15, which maximizes profitability and accounts for approximately half of the total station network. The demonstrated non-linear relationship between infrastructure scaling and profit margins provides operators with concrete design principles for achieving cost-effective deployment of battery swapping networks. The findings highlight that joint consideration of station infrastructure and battery stock levels is essential for effective deployment planning, as uncoordinated expansion may cause underutilization and increased fixed costs.

5.2.5. Sensitivity analysis on different energy management strategies

This experiment evaluates the impact of different energy management strategies on profitability under varying carsharing rental demand scenarios. We compare the following four strategies:

- Strategy 1: plug-in charging only
- Strategy 2: plug-in charging and battery swapping
- Strategy 3: plug-in charging, battery swapping and V2G
- Strategy 4: plug-in charging, battery swapping, V2G and B2G

We analyze these strategies under three rental demand levels: 500, 1000, and 2000 requests. Based on our calculations, the service rate is over 90% for 500 requests, around 70% for 1000 requests, and approximately 40% for 2000 requests. Thus, 500 requests represent a supply-surplus scenario, 1000 requests reflect a moderate-demand scenario, and 2000 requests indicate a supply-shortage scenario. Results are shown in Fig. 14.

Across all four strategies, profit increases with rental demand growth. This is expected since a higher demand enables better utilization of available vehicles and infrastructure, leading to greater revenue. Strategy 4 consistently yields the highest profit, followed by Strategy 3, Strategy 2, and Strategy 1, showing the incremental benefits of adding battery swapping, V2G, and B2G functionalities.

Under the low-demand scenario, where vehicle supply is sufficient, battery swapping does not provide significant additional benefits. Implementing battery swapping in this scenario increases operational costs without substantially improving revenue. However, the introduction of V2G allows more vehicles to participate in electricity sales, potentially enhancing profitability, improving profit by 6.35% compared to Strategy 1. Under both moderate-demand and high-demand scenarios, battery swapping starts to contribute positively, as some vehicles require more efficient recharging methods to meet demand. Battery swapping becomes essential, as seen from the significant profit increase in Strategies 2, 3, and 4 compared to Strategy 1. Notably, in high-demand conditions, adopting battery swapping increases profit by 7.79% over Strategy 1. Therefore, under low-demand conditions, plug-in charging is the most cost-effective option. As demand increases, battery swapping becomes increasingly important and, under high-demand scenarios, significantly enhances both profitability and operational efficiency. Accordingly, energy management strategies should be tailored to expected demand levels, with plug-in charging prioritized at low demand and battery swapping deployed under moderate- and high-demand conditions to ensure vehicle availability and service continuity.

6. Conclusions

In this paper, we propose an integer programming model based on the space-time-energy network to optimize operations in one-way station-based electric carsharing systems with battery swapping, V2G, and B2G integration. The model includes battery swapping operations, charging and selling energy, as well as vehicle relocations, addressing the complex interplay between shared mobility

and energy management. To solve this computationally challenging problem efficiently, we develop a rolling horizon framework combined with a CG-based heuristic algorithm, enabling real-time decision-making under dynamic conditions.

To validate our proposed approach, we conduct experiments using both toy examples and real-world cases, yielding several managerial and operational insights for SEV system operations. The results indicate that systems with limited EV fleet availability or slow charging capabilities exhibit a substantially higher reliance on battery swapping. Accordingly, battery swapping facilities should be prioritized in areas with high demand and constrained fleet coverage, while battery management strategies need to be aligned with charging infrastructure conditions to balance operational efficiency and infrastructure utilization. Furthermore, the implementation of V2G/B2G technologies is shown to be particularly beneficial in fast-charging systems. The results also reveal that, even with an adequately stocked battery supply, an insufficient number of Type 2 stations may lead to reduced profitability, highlighting a trade-off between the number of stocked batteries and the deployment of Type 2 charging stations. Taken together, these findings provide practical guidance for electric carsharing operators to enhance service efficiency and profitability. The proposed framework offers a flexible and scalable decision-support tool that can be readily adapted to real-time operational contexts characterized by multi-factor coupling.

Several directions for future research could extend the scope of this study. First, it would be interesting to incorporate the relocation of stocked batteries between swapping stations into the problem formulation. Second, developing a robust optimization approach that accounts for the inherent uncertainties in travel demand and grid fluctuations would provide more realistic operational strategies. Moreover, while this study optimizes charging and discharging schedules, it does not factor in battery degradation. Thus, developing strategies that mitigate battery degradation during charging and discharging is a direction for further investigation. Finally, as EV adoption accelerates, the interaction between large-scale EV fleets and the power grid presents both opportunities and challenges (Liao et al., 2025). Future research should systematically investigate the integration of EV fleets as distributed energy resources, focusing on their potential roles in electricity market participation and grid stability support.

Declaration of generative AI and AI-assisted technologies in the writing process

During the preparation of this work the authors used ChatGPT in order to improve language. After using this tool, the authors reviewed and edited the content as needed and take full responsibility for the content of the publication.

CRediT authorship contribution statement

Shuang Yang: Conceptualization, Methodology, Validation, Writing – original draft; **Gonçalo Homem de Almeida Correia:** Methodology, Writing – review & editing; **Jianjun Wu:** Supervision, Conceptualization, Funding acquisition; **Huijun Sun:** Supervision, Methodology, Data curation, Project administration.

Data availability

The authors do not have permission to share data.

Acknowledgments

This work is supported by the National Natural Science Foundation of China [grant numbers 72288101, 72361137003], the Postdoctoral Scientific Research Foundation of Beijing Jiaotong University [2025XKBH001], and 111 project. The first author wishes to thank the Department of Transport & Planning, Delft University of Technology, for hosting her in 2022–2023. The authors also acknowledge the China Scholarship Council for supporting the first author.

Appendix A. Proposition and proof

This appendix provides the theoretical justification for the integrality property discussed in Section 4.2.4. We first present a mixed-integer formulation, denoted as [MIP], in which only the variables x_a ($a \in A^{\text{rent}} \cup A^{\text{source}}$) and $g_{i,u}$ are integers, while the others are relaxed to be continuous, as shown below.

[MIP]:

$$\max \sum_{a \in A^{\text{rent}} \cup A^{\text{sell}}} p_a x_a - \sum_{a \in A^{\text{relo}} \cup A^{\text{charg}}} c_a x_a + \sum_{i \in I^{[2]}, u \in U} c_{i,u}^{\text{chain}} g_{i,u} \tag{A.1}$$

s.t. Constraints (2), (4), (5), (16)–(18)

$$x_a \geq 0, \quad \forall a \in A \setminus (A^{\text{rent}} \cup A^{\text{source}}) \tag{A.2}$$

$$x_a, g_{i,u} \in \mathbb{Z}_{\geq 0}, \quad \forall a \in A^{\text{rent}} \cup A^{\text{source}}, i \in I^{[2]}, u \in U \tag{A.3}$$

Proposition 1. There exists an optimal solution to the [MIP] where all decision variables take integer values.

Proof. This proof relies on two theorems related to the totally unimodular matrix, which are briefly introduced below.

Theorem 1. *Each collection of columns of a matrix can be split into two parts so that the sum of the columns in one part minus the sum of the columns in the other part is a vector with entries only 0, 1 and −1, this matrix is totally unimodular (Camion, 1965).*

Theorem 2. *If the coefficient matrix of a linear program is a totally unimodular matrix, and the right-hand side values of the constraints are integers, then the integrality property holds for the linear program (Schrijver, 1998).*

For any given combination of variables (x_a ($a \in A^{\text{rent}} \cup A^{\text{source}}$), $g_{i,u}$), assume this combination can yield feasible solutions for the [MIP]. Now, the remaining decision variables in the [MIP] are x_a ($a \in A^{\text{charg}} \cup A^{\text{sell}} \cup A^{\text{idle}} \cup A^{\text{relo}}$). For simplicity, we denote $A^{[1]} = A^{\text{charg}} \cup A^{\text{sell}} \cup A^{\text{idle}} \cup A^{\text{relo}}$, denote $A^{[2]} = A^{\text{charg}} \cup A^{\text{sell}} \cup A^{\text{idle}}$, denote $\sum_{a \in A^{\text{rent}}} p_a x_a + \sum_{i \in I^{[2]}, u \in U} c^{\text{chain}}_{i,u} g_{i,u}$ as ψ, and denote $\sum_{a \in \zeta^+_{i,t,e} \cap A^{\text{rent}}} x_a + \sum_{u \in U, a \in \zeta^+_{i,t,e} \cap A^{\text{swap}}} \delta^a_{i,u} g_{i,u} - \sum_{a \in \zeta^-_{i,t,e} \cap A^{\text{rent}}} x_a - \sum_{u \in U, a \in \zeta^-_{i,t,e} \cap A^{\text{swap}}} \delta^a_{i,u} g_{i,u}$ as $\gamma_{i,t,e}$. We consider the following problem:

$$L_{(x_{a(a \in A^{\text{rent}} \cup A^{\text{source}})}, g_{i,u})} = \max \sum_{a \in A^{\text{sell}}} p_a x_a - \sum_{a \in A^{\text{relo}} \cup A^{\text{charg}}} c_a x_a + \psi \tag{A.4}$$

$$\text{s.t.} \quad \sum_{a \in \zeta^+_{i,t,e} \cap A^{[1]}} x_a - \sum_{a \in \zeta^-_{i,t,e} \cap A^{[1]}} x_a = -\gamma_{i,t,e}, \quad \forall i \in I, t \in T^{[1]}, e \in E \tag{A.5}$$

$$\sum_{a \in A^{\text{start}}_{i,t} \cap A^{[2]}} x_a \le m_i - \sum_{u \in U, a = (n_{i,t,0}, n_{i,t+1,|E|}) \in A^{\text{swap}}} \delta^a_{i,u} g_{i,u}, \quad \forall i \in I, t \in T \tag{A.6}$$

$$x_a \ge 0, \quad \forall a \in A^{[1]} \tag{A.7}$$

Given specific values of x_a ($a \in A^{\text{rent}} \cup A^{\text{source}}$) and $g_{i,u}$, then ψ, $\gamma_{i,t,e}$, and $m_i - \sum_{u \in U, a = (n_{(i,t,0)}, n_{(i,t+1,|E|)}) \in A^{\text{swap}}} \delta^a_{i,u} g_{i,u}$ are fixed and must be integers. The coefficient matrix of the above model can be represented as $\begin{bmatrix} \mathbf{C} \\ \mathbf{D} \quad \mathbf{0} \end{bmatrix}$, where $\mathbf{C}$ corresponds to the coefficients of variables x_a ($a \in A^{[1]}$) in Constraints (A.5), $\begin{bmatrix} \mathbf{D} & \mathbf{0} \end{bmatrix}$ corresponds to the coefficients of variables x_a ($a \in A^{[1]}$) in Constraints (A.6), $\mathbf{D}$ represents the coefficients of x_a ($a \in A^{[2]}$) in Constraints (A.6), and $\mathbf{0}$ represents the coefficients of x_a ($a \in A^{\text{relo}}$) in Constraints (A.6). $\mathbf{C}$ can be regarded as the adjacency matrix of the minimum most network flow problem, in which each column contains a single 1 and a single −1, with all other elements being 0. For $\mathbf{D}$, each column contains a single 1, with all other elements being 0. The coefficient matrix in this model can be divided into two parts: $\mathbf{C}$ corresponds to the first part, and $\begin{bmatrix} \mathbf{D} & \mathbf{0} \end{bmatrix}$ corresponds to the second part. The sum of each column in one part minus the sum of each column in the other part is a vector with entries only 0, and -1. According to Theorem 1, this matrix is totally unimodular. As per Theorem 2, the optimal solution for this model is guaranteed to be integers. Each combination $(x_{a(a \in A^{\text{rent}} \cup A^{\text{source}})}, g_{i,u})$ corresponds to a $L_{(x_{a(a \in A^{\text{rent}} \cup A^{\text{source}})}, g_{i,u})}$. Solving the [MIP] is equivalent to find $\left(x_{a(a \in A)}, g_{i,u}\right) \in \arg\max \left\{ L_{(x_{a(a \in A^{\text{rent}} \cup A^{\text{source}})}, g_{i,u})} \right\}$. With this, the proof is complete, demonstrating that solving the [MIP] yields an integer optimal solution. □

References

Agatz, N. A.H., Erera, A.L., Savelsbergh, M. W.P., Wang, X., 2011. Dynamic ride-sharing: a simulation study in metro atlanta. Transp. Res. Part B: Methodol. 45, 1450–1464.

Ait-Ouahmed, A., Josselin, D., Zhou, F., 2018. Relocation optimization of electric cars in one-way car-sharing systems: modeling, exact solving and heuristics algorithms. Int. J. Geographical Inf. Sci. 32 (2), 367–398.

Albrechtowicz, P., 2023. Electric vehicle impact on the environment in terms of the electric energy source-case study. Energy Rep. 9, 3813–3821.

Bekli, S., Boyacı, B., Zografos, K.G., 2021. Enhancing the performance of one-way electric carsharing systems through the optimum deployment of fast chargers. Transp. Res. Part B: Methodol. 152, 118–139.

Boyacı, B., Zografos, K.G., Geroliminis, N., 2015. An optimization framework for the development of efficient one-way car-sharing systems. Eur. J. Oper. Res. 240 (3), 718–733.

Brandstätter, G., Kahr, M., Leitner, M., 2017. Determining optimal locations for charging stations of electric car-sharing systems under stochastic demand. Transp. Res. Part B: Methodol. 104, 17–35.

Caggiani, L., Prencipe, L.P., Ottomanelli, M., 2021. A static relocation strategy for electric car-sharing systems in a vehicle-to-grid framework. Transp. Lett. 13 (3), 219–228.

Camion, P., 1965. Characterization of totally unimodular matrices. Proc. Am. Math. Soc. 16 (5), 1068–1073.

Chang, X., Wu, J., de Almeida Correia, G.H., Sun, H., Feng, Z., 2022. A cooperative strategy for optimizing vehicle relocations and staff movements in cities where several carsharing companies operate simultaneously. Transp. Res. Part E: Logist. Transp. Rev. 161, 102711.

Chen, Y., Liu, Y., 2023. Integrated optimization of planning and operations for shared autonomous electric vehicle systems. Transp. Sci. 57 (1), 106–134.

Chenlei, L., Xiqun (Michael), C., Ziyou, G., 2025. Toward smart charging, synergistic infrastructure and storable grid for coordinated power and transportation systems. Front. Eng. Manag. 12 (3), 704–709, https://doi.org/10.1007/s42524-025-5054-6.

Cordeau, J.-F., Dell'Amico, M., Falavigna, S., Iori, M., 2015. A rolling horizon algorithm for auto-carrier transportation. Transp. Res. Part B: Methodol. 76, 68–80.

Cui, D., Wang, Z., Liu, P., Wang, S., Dorrell, D.G., Li, X., Zhan, W., 2023. Operation optimization approaches of electric vehicle battery swapping and charging station: a literature review. Energy 263, 126095.

Di Febbraro, A., Sacco, N., Saeednia, M., 2019. One-way car-sharing profit maximization by means of user-based vehicle relocation. IEEE Trans. Intell. Transp. Syst. 20 (2), 628–641.

Du, J.Y., Brunner, J.O., Kolisch, R., 2014. Planning towing processes at airports more efficiently. Transp. Res. Part E: Logist. Transp. Rev. 70, 293–304.

Freund, D., Raab, A.F., Küster, T., Albayrak, S., Strunz, K., 2012. Agent-based integration of an electric car sharing fleet into a smart distribution feeder. In: 2012 3rd IEEE PES Innovative Smart Grid Technologies Europe (ISGT Europe). IEEE, pp. 1–8.

Gambella, C., Malaguti, E., Masini, F., Vigo, D., 2018. Optimizing relocation operations in electric car-sharing. Omega 81, 234–245.

He, P., Jin, J.G., Schulte, F., Trépanier, M., 2023. Optimizing first-mile ridesharing services to intercity transit hubs. Transp. Res. Part C: Emerging Technol. 150, 104082.

Huang, K., de Almeida Correia, G.H., An, K., 2018. Solving the station-based one-way carsharing network planning problem with relocations and non-linear demand. Transp. Res. Part C: Emerging Technol. 90, 1–17.

Iacobucci, R., McLellan, B., Tezuka, T., 2019. Optimization of shared autonomous electric vehicles operations with charge scheduling and vehicle-to-grid. Transp. Res. Part C: Emerging Technol. 100, 34–52.

Jamshidi, H., Correia, G. H.A., van Essen, J.T., Nökel, K., 2021. Dynamic planning for simultaneous recharging and relocation of shared electric taxies: a sequential MILP approach. Transp. Res. Part C: Emerging Technol. 125, 102933.
Jordehi, A.R., Javadi, M.S., Catalão, J. P.S., 2020. Energy management in microgrids with battery swap stations and var compensators. J. Clean. Prod. 272, 122943.
Jorge, D., Molnar, G., de Almeida Correia, G.H., 2015. Trip pricing of one-way station-based carsharing networks with zone and time of day price variations. Transp. Res. Part B: Methodol. 81, 461–482.
Kek, A. G.H., Cheu, R.L., Meng, Q., Fung, C.H., 2009. A decision support system for vehicle relocation operations in carsharing systems. Transp. Res. Part E: Logist. Transp. Rev. 45 (1), 149–158.
Levin, M.W., Odell, M., Samarasena, S., Schwartz, A., 2019. A linear program for optimal integration of shared autonomous vehicles with public transit. Transp. Res. Part C: Emerging Technol. 109, 267–288.
Li, Q., Zhao, D., Li, X., Wang, X., 2022. Electric vehicle sharing based “energy sponge” service interfacing transportation and power systems. Cleaner Logist. Supply Chain 3, 100022.
Li, X., Ma, J., Cui, J., Ghiasi, A., Zhou, F., 2016. Design framework of large-scale one-way electric vehicle sharing systems: a continuum approximation model. Transp. Res. Part B: Methodol. 88, 21–45.
Liang, X., de Almeida Correia, G.H., An, K., van Arem, B., 2020. Automated taxis’ dial-a-ride problem with ride-sharing considering congestion-based dynamic travel times. Transp. Res. Part C: Emerging Technol. 112, 260–281.
Liao, Z., Taiebat, M., Xu, M., 2021. Shared autonomous electric vehicle fleets with vehicle-to-grid capability: economic viability and environmental co-benefits. Appl. Energy 302, 117500.
Liu, Y., Xie, J., Chen, N., 2022. Stochastic one-way carsharing systems with dynamic relocation incentives through preference learning. Transp. Res. Part E: Logist. Transp. Rev. 166, 102884.
Lu, R., de Almeida, C. G.H., Zhao, X., Liang, X., Lv, Y., 2021. Performance of one-way carsharing systems under combined strategy of pricing and relocations. Transp. B: Transport Dyn. 9 (1), 134–152.
Mahoor, M., Hosseini, Z.S., Khodaei, A., 2019. Least-cost operation of a battery swapping station with random customer requests. Energy 172, 913–921.
Marufuzzaman, M., Gedik, R., Roni, M.S., 2016. A benders based rolling horizon algorithm for a dynamic facility location problem. Comput. Ind. Eng. 98, 462–469.
Montoya, A., Guéret, C., Mendoza, J.E., Villegas, J.G., 2017. The electric vehicle routing problem with nonlinear charging function. Transp. Res. Part B: Methodol. 103, 87–110.
Mounce, R., Nelson, J.D., 2019. On the potential for one-way electric vehicle car-sharing in future mobility systems. Transp. Res. Part A: Policy Pract. 120, 17–30.
Noel, L., Zarazua, G., Rubens, D.E., Kester, J., Sovacool, B.K., 2019. Vehicle-to-grid a sociotechnical transition beyond electric mobility. Energy, climate and the environment. Palgrave Macmillan Cham. https://doi.org/10.1007/978-3-030-04864-8.
Nourinejad, M., Roorda, M.J., 2014. A dynamic carsharing decision support system. Transp. Res. Part E: Logist. Transp. Rev. 66, 36–50.
Nourinejad, M., Zhu, S., Bahrami, S., Roorda, M.J., 2015. Vehicle relocation and staff rebalancing in one-way carsharing systems. Transp. Res. Part E: Logist. Transp. Rev. 81, 98–113.
Pelletier, S., Jabali, O., Laporte, G., Veneroni, M., 2017. Battery degradation and behaviour for electric vehicles: review and numerical analyses of several models. Transp. Res. Part B: Methodol. 103, 158–187.
Prencipe, L.P., Van Essen, J.T., Caggiani, L., Ottomanelli, M., de Almeida Correia, G.H., 2022. A mathematical programming model for optimal fleet management of electric car-sharing systems with vehicle-to-grid operations. J. Clean Prod. 368, 133147.
Ren, S., Luo, F., Lin, L., Hsu, S.-C., Li, X.I., 2019. A novel dynamic pricing scheme for a large-scale electric vehicle sharing network considering vehicle relocation and vehicle-grid-integration. Int. J. Prod. Econ. 218, 339–351.
Revankar, S.R., Kalkhambkar, V.N., 2021. Grid integration of battery swapping station: a review. J. Energy Storage 41, 102937.
Rupp, M., Handschuh, N., Rieke, C., Kuperjans, I., 2019. Contribution of country-specific electricity mix and charging time to environmental impact of battery electric vehicles: a case study of electric buses in germany. Appl. Energy 237, 618–634.
Santos, G. G.D., de Almeida Correia, G.H., 2019. Finding the relevance of staff-based vehicle relocations in one-way carsharing systems through the use of a simulation-based optimization tool. J. Intell. Transp. Syst. 23 (6), 583–604.
Santos, G. G.D., Birolini, S., de Almeida Correia, G.H., 2023. A space–time-energy flow-based integer programming model to design and operate a regional shared automated electric vehicle (SAEV) system and corresponding charging network. Transp. Res. Part C: Emerging Technol. 147, 103997.
Schrijver, A., 1998. Theory of Linear and Integer Programming. John Wiley & Sons.
Shaker, M.H., Farzin, H., Mashhour, E., 2023. Joint planning of electric vehicle battery swapping stations and distribution grid with centralized charging. J. Energy Storage 58, 106455.
Shui, C.S., Szeto, W.Y., 2018. Dynamic green bike repositioning problem - a hybrid rolling horizon artificial bee colony algorithm approach. Transp. Res. Part D: Transport Environ. 60, 119–136.
Stokkink, P., Geroliminis, N., 2021. Predictive user-based relocation through incentives in one-way car-sharing systems. Transp. Res. Part B: Methodol. 149 (C), 230–249.
Sturmberg, B. C.P., Hapuarachchi, L., Jones, L., Lucas-Healey, K., van Biljon, J., 2024. Vehicle-to-grid response to a frequency contingency in a national grid. NPJ Sustain. Mobility Transport 1 (1), 7.
Uhrig, M., Weiß, L., Suriyah, M., Leibfried, T., 2015. E-mobility in car parks–guidelines for charging infrastructure expansion planning and operation based on stochastic simulations. In: Evs28 International Electric Vehicle Symposium and Exhibition, pp. 1–12.
Van Fan, Y., Jiang, P., Klemeš, J.J., Ocłoń, P., 2022. Minimum environmental footprint charging of electric vehicles: a spatiotemporal scenario analysis. Energy Convers. Manage. 258, 115532.
Wang, L., Xu, M., Qin, H., 2023. Joint optimization of parcel allocation and crowd routing for crowdsourced last-mile delivery. Transp. Res. Part B: Methodol. 171, 111–135.
Wang, N., Jia, S., Liu, Q., 2021. A user-based relocation model for one-way electric carsharing system based on micro demand prediction and multi-objective optimization. J. Clean Prod. 296, 126485.
Wang, Y., Lai, K., Chen, F., Li, Z., Hu, C., 2019. Shadow price based co-ordination methods of microgrids and battery swapping stations. Appl. Energy 253, 113510.
Wang, Z., Hou, S., 2023. A real-time strategy for vehicle-to-station recommendation in battery swapping mode. Energy 272, 127154.
Wenlong, S., Haibo, C., David, W., Washington, O., 2023. How far are we from the large-scale adoption of V2G technology?. Eng. Manag. 13 (1), 240–245. https://doi.org/10.1103/PhysRevLett.127.111803.
Wu, H., 2022. A survey of battery swapping stations for electric vehicles: operation modes and decision scenarios. IEEE Trans. Intell. Transp. Syst. 23 (8), 10163–10185.
Wu, W., Lin, Y., Liu, R., Jin, W., 2022. The multi-depot electric vehicle scheduling problem with power grid characteristics. Transp. Res. Part B: Methodol. 155, 322–347.
Xiao, L., Zhen, L., Laporte, G., Baldacci, R., Wang, C., 2022. A column generation-based heuristic for a rehabilitation patient scheduling and routing problem. Comput. Oper. Res. 148, 105970.
Xu, M., Meng, Q., 2019. Fleet sizing for one-way electric carsharing services considering dynamic vehicle relocation and nonlinear charging profile. Transp. Res. Part B: Methodol. 128, 23–49.
Xu, M., Meng, Q., Liu, Z., 2018. Electric vehicle fleet size and trip pricing for one-way carsharing services considering vehicle relocation and personnel assignment. Transp. Res. Part B: Methodol. 111, 60–82.
Xu, M., Yang, H., Wang, S., 2020. Mitigate the range anxiety: siting battery charging stations for electric vehicle drivers. Transp. Res. Part C: Emerging Technol. 114, 164–188.
Yang, S., Wu, J., Sun, H., Qu, Y., Li, T., 2021a. Double-balanced relocation optimization of one-way car-sharing system with real-time requests. Transp. Res. Part C: Emerging Technol. 125, 103071.

Yang, X., Shao, C., Zhuge, C., Sun, M., Wang, P., Wang, S., 2021b. Deploying battery swap stations for shared electric vehicles using trajectory data. Transp. Res. Part D: Transport Environ. 97, 102943.
Yao, Z., Gendreau, M., Li, M., Ran, L., Wang, Z., 2022. Service operations of electric vehicle carsharing systems from the perspectives of supply and demand: a literature review. Transp. Res. Part C: Emerging Technol. 140, 103702.
You, P., Low, S.H., Tushar, W., Geng, G., Yuen, C., Yang, Z., Sun, Y., 2018. Scheduling of EV battery swapping-Part I: centralized solution. IEEE Trans. Control Netw. Syst. 5 (4), 1887–1897.
Zhan, W., Wang, Z., Zhang, L., Liu, P., Cui, D., Dorrell, D.G., 2022. A review of siting, sizing, optimal scheduling, and cost-benefit analysis for battery swapping stations. Energy 258, 124723.
Zhang, D., Liu, Y., He, S., 2019. Vehicle assignment and relays for one-way electric car-sharing systems. Transp. Res. Part B: Methodol. 120, 125–146.
Zhang, S., Sun, H., Wang, X., Lv, Y., Wu, J., 2022. Optimization of personalized price discounting scheme for one-way station-based carsharing systems. Eur. J. Oper. Res. 303 (1), 220–238.
Zhang, Y., Lu, M., Shen, S., 2021. On the values of vehicle-to-grid electricity selling in electric vehicle sharing. Manuf. Serv. Oper. Manage. 23 (2), 488–507.
Zhao, D., Li, X., Cui, J., 2021. A simulation-based optimization model for infrastructure planning for electric autonomous vehicle sharing. Comput.-Aided Civ. Infrastruct. Eng. 36 (7), 858–876.
Zhao, M., Li, X., Yin, J., Cui, J., Yang, L., An, S., 2018. An integrated framework for electric vehicle rebalancing and staff relocation in one-way carsharing systems: model formulation and lagrangian relaxation-based solution approach. Transp. Res. Part B: Methodol. 117, 542–572.
Zhen, L., Tan, Z., de Koster, R., Wang, S., 2023. How to deploy robotic mobile fulfillment systems. Transp. Sci. 57 (6), 1671–1695.
Zhou, J., Xu, X., Long, J., Ding, J., 2022. Metro crew planning with day-off pattern, duty type, and rostering scheme considerations. Transp. Res. Part C: Emerging Technol. 143, 103832.